INTERNATIONAL JOURNAL OF
APPLIED SCIENCES (IJAS)

INTERNATIONAL JOURNAL OF APPLIED SCIENCES (IJAS)

VOLUME 2, ISSUE 3, 2011

EDITED BY
DR. NABEEL TAHIR

INTERNATIONAL JOURNAL OF APPLIED SCIENCES (IJAS)

CSC Publishers, 2011

EDITORIAL PREFACE

This is first issue of volume two of the International Journal of Applied Sciences (IJAS). IJAS is an International refereed journal for publication of current research in applied sciences. IJAS publishes research papers dealing primarily with the research aspects of Applied Sciences in general. Publications of IJAS are beneficial for researchers, academics, scholars, advanced students, practitioners, and those seeking an update on current experience, state of the art research theories and future prospects in relation to applied science. Some important topics covers by IJAS are agriculture, architectural, audio, automotive, military ammunition, military technology, military etc.

The initial efforts helped to shape the editorial policy and to sharpen the focus of the journal. Starting with volume 2, 2011, IJAS appears in more focused issues. Besides normal publications, IJAS intend to organized special issues on more focused topics. Each special issue will have a designated editor (editors) – either member of the editorial board or another recognized specialist in the respective field.

This journal publishes new dissertations and state of the art research to target its readership that not only includes researchers, industrialists and scientist but also advanced students and practitioners. IJAS seeks to promote and disseminate knowledge in the applied sciences, natural and social sciences industrial research materials science and technology, energy technology and society including impacts on the environment, climate, security, and economy, environmental sciences, physics of the games, creativity and new product development, professional ethics, hydrology and water resources, wind energy.

IJAS editors understand that how much it is important for authors and researchers to have their work published with a minimum delay after submission of their papers. They also strongly believe that the direct communication between the editors and authors are important for the welfare, quality and wellbeing of the Journal and its readers. Therefore, all activities from paper submission to paper publication are controlled through electronic systems that include electronic submission, editorial panel and review system that ensures rapid decision with least delays in the publication processes.

To build its international reputation, we are disseminating the publication information through Google Books, Google Scholar, Directory of Open Access Journals (DOAJ), Open J Gate, ScientificCommons, Docstoc, Scribd, CiteSeerX and many more. Our
International Editors are working on establishing ISI listing and a good impact factor for IJAS. We would like to remind you that the success of our journal depends directly on the number of quality articles submitted for review. Accordingly, we would like to request your participation by submitting quality manuscripts for review and encouraging your colleagues to submit quality manuscripts for review. One of the great benefits we can provide to our prospective authors is the mentoring nature of our review process. IJAS provides authors with high quality, helpful reviews that are shaped to assist authors in improving their manuscripts.

Editorial Board Members
International Journal of Applied Sciences (IJAS)

TABLE OF CONTENTS

Volume 2, Issue 3, August 2011

Pages

Mehrbakhsh Nilashi, Othman bin Ibrahim, Amir Talebi & Alireza Khoshraftar

Examining the Relationship of Emotional Intelligence and Organizational Effectiveness

Mehrbakhsh Nilashi   *Nilashidotnet@yahoo.com*
Computer Engineering Department
Islamic Azad University of Roudsar and Amlash
Roudsar, Iran

Othman Bin Ibrahim   *Othmanibrahim@utm.my*
Faculty of Computer Science and Information Systems
University Teknologi Malaysia
Johor, Malaysia

Amir Talebi   *Amirtalebi@gmail.com*
Faculty of Computer Science and Information Systems
University Teknologi Malaysia
Johor, Malaysia

Alireza Khoshraftar   *Ali_samick@yahoo.com*
Faculty of Computer Science and Information Systems
University Teknologi Malaysia
Johor, Malaysia

Abstract

The director of an organization needs special features to adapt the organization with changes in order to survive and grow in new environments, that almost all managers find it difficult to address such issues. One of the important features that can help the directors and the managers to respond to such changes is the emotional intelligence factor. The goal of this research is to evaluate the relation between the emotional structure of an organization (called emotional intelligence) and the organizational effectiveness. Both, graphical and statistical modeling was used as a guide in the research, and also standardized questions are used in both, emotional intelligence and organizational effectiveness issues. The statistical population of this research includes the managers, assistants and the executive region manager of Rasht municipality, which 240 people were chosen as a sample from them. Over 80% of the respondents have BA and higher education and the majority of respondents (80%) have the job experience with less than 12 years. the analysis of the major and minor hypothesis were done by statistical software such as: STATISTICA, SPSS and EXCEL. The outcomes revealed the meaningful relation between the emotional intelligence and the organizational effectiveness and also, it is recognized, in this research that the motivation component has the most influential role on the organizational effectiveness.

Keywords: Emotional Intelligence, Organizational Effectiveness, Self-awareness, Self-Management, Sympathy, Social Skills.

1. INTRODUCTION

Every leader or manager of an organization, in order to achieve his or her goals, needs to be aware of the forces, feelings and motivations of his/her staff. We utilize such awareness in our work and life to achieve the best results. Unfortunately, some times we are afraid to show our feelings because we don't know how effective they might be [1].

One way to grasp these feelings and utilize them effectively at work is to recognize and understand emotional intelligence. Development and deep reflection regarding emotional

Mehrbakhsh Nilashi, Othman bin Ibrahim, Amir Talebi & Alireza Khoshraftar

intelligence and using its entire elements can increasingly, improve the organizational – relationships, the staff co- operation and the exploitation of social skills. [2] The quality of a person to guidance and support the goals of an organization is that, the staff feel, they have an important role in an individual and organizational development [3]. The failure and frustration risk in goals fulfillment in the organizations that don't use the emotional intelligence principle, is higher, in contrast to the organizations that use this principle in their sources.

The ruling culture in these organizations prevents the staff to represent their useful criticisms and/or to encourage the secrecy and cordial relations inside the organizations.

The organizations that institutionalize emotional intelligence's elements in their human sources, indeed they allow an expressed culture rules in the organizations, of course within the frame work of the organizational laws. And the staff can represent their criticisms and proposals bravely and feel sympathy within the organization [4].

Goleman believes if someone has an ability to recognize his or her feeling and emotions and knows how to use these things as a tool, he/she will be able to make good decisions, manage his/her relations, create motivation for his/her self or for others, be hopeful in bad and difficult situations, control his/her stress and to create sympathy within the other organization's staff [3].

Most of the variables, but not all of them can be numerical. Analytical tools can provide the most part of the data that are required for a consistent and clear image, but always there is ambiguity, approximate estimation and conjecture. An important thing to mention is that the leader of an organization has to trust his feeling. Such feelings are often in a right direction and sometimes in a wrong one. The leaders that often feel that they are in a right direction have a good sense about this case that why they act like this. They have learned to distinguish between the wrong feelings and the purposeful feelings. In other words, emotional intelligence helps them to change to leaders that most of their decisions are fraught with helpfulness, correctness, usefulness and carefulness [5].

Emotional intelligence has an influence over recruiting the intelligent people. A statistics organization's research that was conducted over two millions staff within 700 companies, revealed that, the duration that a staff remains at a company , or the amount of his efficiency output is determined by the direct relation between him/her and his/her supervisor [5].

The other research that was conducted by Espiron, showed this effect in a simple way. He, as a staff and an advisor for three American companies, showed that just 11% of the staff that appraised their manager, said, they were going to have another job next year. Any how, 40% of the staff that evaluated the performance of the manager as weak, decided to give up their job.

In other words, the resignation probability of the staff that have a good manager, in contrast to the staff that has weak manager is four times less. [6]

The study of the research background and the classification of them, showed, that the majority of the researches that have been conducted regarding emotional intelligence in organizations, focused on the way of effectiveness [7], improvement of the managers effectiveness, [7] the success of a group work [3] innovation and solving problem [8] the staff motivation [8] making a good decision [9] and the staff efficiency [10].

2. RESEARCH IMPORTANCE
What makes this research important is that no one has dealt with the organizational effectiveness factor from the emotional intelligence point of view as an important factor in human resource. The other important point that has been done in this research is that the majority of the researches conducted in emotional intelligence field

Was regarding the staff efficiency, workforce productivity, sales increase, and increase in the workgroup efficiency but in this research, the researcher is trying to investigate the effect of emotional intelligence of a group of staff over their total output.

The other important point in this research is dealing with the organizations that profitability is not defined as an evaluation criteria in them in fact the duty and mission of the Rasht municipality regions considered as a statistical society and they are not profit – making. This subject is new in the accomplished research.

3. RESEARCH OBJECTIVES
The goal of this research is to introduce the human feelings in staff that nobody pays attention to it, and study the relations between this human factor to materialize the goals and the organization's strategies for the first time .Thus, the objectives of this research are as follows:
- To recognize the levels of the emotional intelligence factors (self – awareness, social awareness and connecting skills) between the respondents and the organizational effectiveness level.
- To determine the relation between the emotional intelligence grade and organizational effectiveness.
- To recognize the emotional intelligence factor that has the most effect on the organizational effectiveness.

4. RESEARCH THEORIES
Based on Peter Saloy's model, six theories have been studied in this research. That the major theory was about the study of the relation between the whole emotional intelligence and the effectiveness, and other five theories compared the relation between every part of the emotional intelligence and organizational effectiveness that include (self-awareness, self-management, self-motivation, sympathy and connecting skills). The graphical model of the relation between emotional intelligence and organizational effectiveness is shown in Fig 1.
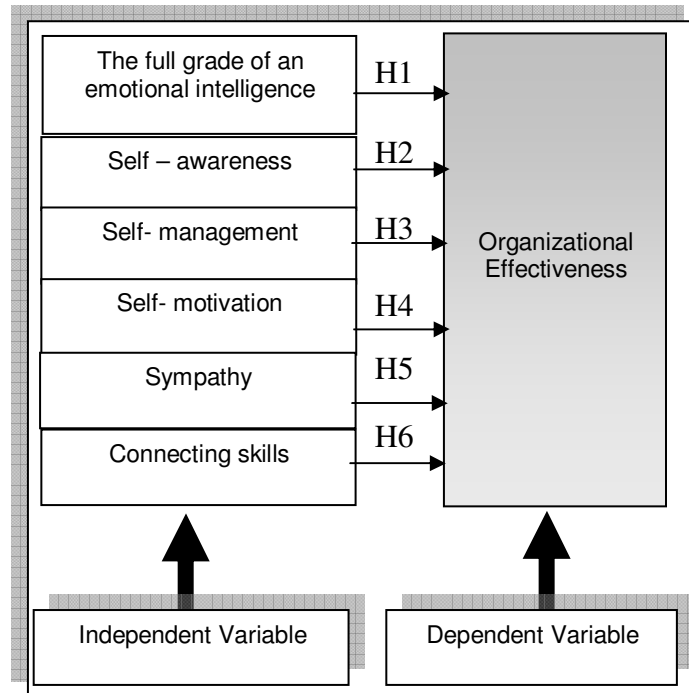
FIGURE 1: The graphical model of the relation between emotional intelligence and organizational effectiveness.

- There is a meaningful relation between the organization's staff emotional intelligence and organizational effectiveness.
- There is a meaningful relation between the self-awareness factor the staff and organizational effectiveness.
- There is a meaningful relation between the self-management factor of the staff and the organizational effectiveness.
- There is a meaningful relation between the self-motivation factor of the staff and the organizational effectiveness.
- There is a meaningful relation between the sympathy factor of the staff and the organizational effectiveness.
- There is a meaningful relation between the connecting skills factor of the staff and the organizational effectiveness.

5. RESEARCH METHODOLOGY

According to the goal of this research, this study is a research based on the correlation by using the selected simple case by case study in Rasht municipality and elective samples has been from the executive regions.

They used two standard questionnaires, in order to collect the required data for this research that the first one is for measuring the emotional intelligence and the second one is for measuring the organizational effectiveness. For being sure of the correctness of these questionnaires, both of them are tested orally and the outcome showed a suitable narrative and enduring. At the end, as hypothesis test, the data analyzed statistically. The researchers choose the statistical society by his (her) knowledge from the executive regions in Rasht municipality and studied the managers and the positions of the Rasht municipality and the elder staff sample that have been choose by chance. All the examined samples were 240 people. The statistical societies that have been chosen in this research were all the regions manager and assistants, the elder leaders and staff from the 3 parts in Rasht municipality that consist of 300 people.

For better understanding about the structure and the nature of the statistical society at first the organizational structure for each region has been drawn like as followed each one of these 3 regions is like a category for the choose sample.

For society survey , the sample that include 240 people derived from a regions that are like a category and by attention to the equivalence between the society number in each region , the sample by 20 people derived from each region by considering :

$$\alpha = 5\% \quad , \quad p = 0.5 \quad , \quad d = 0.05 \quad , \quad N = 650$$

We have in formula 1 that is known as Kokaran formula:

$$n_0 = \frac{z_{\frac{\alpha}{2}}^2 p(1-p)}{d^2} = \frac{1.96^2 \times 0.5 \times 0.5}{0.05^2} = 384.16 \qquad (1)$$

$$n = \frac{n_0}{1+\frac{n_0}{N}} = \frac{384.16}{1+\frac{384.16}{640}} \approx 240$$

This study is a research based on the correlations, by using the selected sample. So we can consider it as a functional research. The tool of this research includes two questionnaires. One of them examines the affective intelligence and the other, study the organizational effectiveness. We introduced each of these questionnaires in brief.

6. EMOTIONAL EFFECTIVENESS QUESTIONNAIRE

This questionnaire was designed by H.Vizinger and introduced as an affective intelligence in his book. It is based on the Salvy's Fire- dimensional model. The questionnaire includes 25 questions that totally measured the people's affective intelligence. Any person can take grade between 25 to 125, that the grade below 50 shows the low affective intelligence, between 50 to 100 shows the average affective intelligence and over 100 shows the high affective intelligence of people.

Fire dimensions of the emotional intelligence examined in this questionnaire as followed:

- The total questions grade 1, 6, 11, 16, 21, shows the rate of the self-awareness.
- The total questions grade 2, 7, 12, 17, 22, shows the rate of the self-management.
- The total questions grade 3, 8,13,18,23, shows the rate of the motivation.
- The total questions grade 4, 9,14,19,24, shows the rate of the sympathy.

The total questions grade 5, 10,15,20,25, shows the rate of the social skills.

7. ORGANIZATIONAL EFFECTIVENESS QUESTIONNAIRE

This questionnaire was based on the goal's approach and the human sources approach that was designed by the professional management borganization1. In this questionnaire the following issue described as indexes for determining the organizational effectiveness.

This questionnaire consists of 17 questions and each person can take the grade between 11 to 85. The grade that is below 34 shows the low effectiveness, between 35 to 68 shows the average effectiveness and over 68 shows the high effectiveness.

- The structure of the questions in the planned questionnaire includes the following fields:
- The organization view and mission. (Include the questions 1 and 2)
- The organization goals. (include the question 3 to 6)
- Duty and responsibilities. (Include the questions 7 to 9)
- The staff welfare.(include the questions 10 and 11)
- The organization's process.(question number 12)
- Connections (questions number 13 and 14)
- Clients (include the questions 15 to 17)

Narrative and enduring are the factors that must be discussed for any measuring evaluation tool.

The questionnaires that used in this research were the reliable questionnaires and their validity confirmed in several research.

In this research, they used the Psychology and management authority's view, for determining the narrative in both questionnaires and by attention to the gathered view, both questionnaires have formal narrative. At first in this research, they used the psychology and management authority's view, for determining the narrative in both questionnaires and by attention to the gathered view, both questionnaires have formal narrative. At first, they used descriptive way for the questionnaires enduring. In this way, the questions divided in two groups by chance and correlation ratio between the outcomes of these two groups was estimated.

They choose 20 units of managers, assistants and elder staff for evaluate the enduring and each of them completed the research questionnaire. Then the questions of each questionnaire divided in two groups by STATISTICA software, accidentally and the result for the affective intelligence questionnaire equal to 83% and for the organizational effectiveness, it equals to 79% that is showed the high enduring in research questionnaires.

After receiving all the answer sheets, again the enduring of both questionnaires was evaluated by the software and the result for the emotional intelligence questionnaire equal to 844% and for the

effectiveness questionnaire equal to 811% that like the firs outcomes showed the high enduring. The enduring calculations showed in table 1 and 2:

N of Items	Cronbach's Alpha
25	.844

TABLE 1: the calculations of the validity evaluation in intelligence questionnaire

N of Items	Cronbach's Alpha
17	.811

TABLE 2: the calculations of the validity evaluation in effectiveness questionnaire

8. RESULTS AND INTERPRETATION OF QUESTIONNAIRES

The data that was collected and classified by a questionnaire and interview was used as a major source for gaining new information about the subject to study phenomenon. They used descriptive statistics and inferential statistics ways for analyzing the gathered data. They used descriptive statistics for summarizing the gathered data about the society. Note that the goal of the descriptive statistics is not justification, but to describe and extract the main points and fulfill the data combinations in the form of the present condition. Also, they used statistical software like STATISTICA, SPSS, and EXCEL, to analyze and classify the main and minor hypothesis outcomes of the research.

9. SURVEY THE EMOTIONAL INTELLIGENCE OF THE RESPONDENTS.

9.1. Distribution of the Sample Plenty in the Dimension of the Self-Awareness rate.

Based on the table3, 87.1% of the respondents get the high grade in the rate of the self-awareness and 12.9% get the average grade and 1.7% gets the lowest grade in this dimension by considering the grade between 5 to 25 for answering to the dimension in total, the average value that gained for the self-awareness is 20.2.

The rate of the self-awareness	plenty	The percent of the plenty	The gathering plenty	The percent of the gathering plenty
Less than 8	0	0.0%	0	0.0%
8to 12	4	1.7%	4	1.7%
13 to 17	27	11.3%	31	12.9%
18to 22	159	66.3%	190	79.2%
23 and more	50	20.8%	240	100.0%
Total	240	100%	-	-

The rate of the self-awareness	plenty	The percent of the plenty	The gathering plenty	The percent of the gathering plenty
Less than 8	0	0.0%	0	0.0%
8to 12	11	4.6%	11	4.6%
13 to 17	80	33.3%	91	37.9%
18to 22	131	54.6%	222	92.5%
23 and more	18	7.5%	240	100.0%
Total	240	100%	-	-
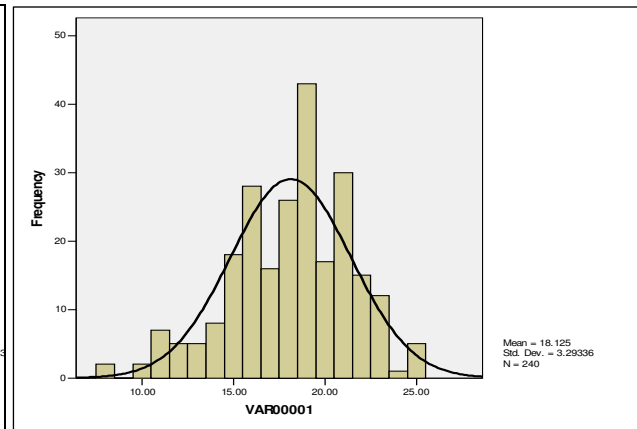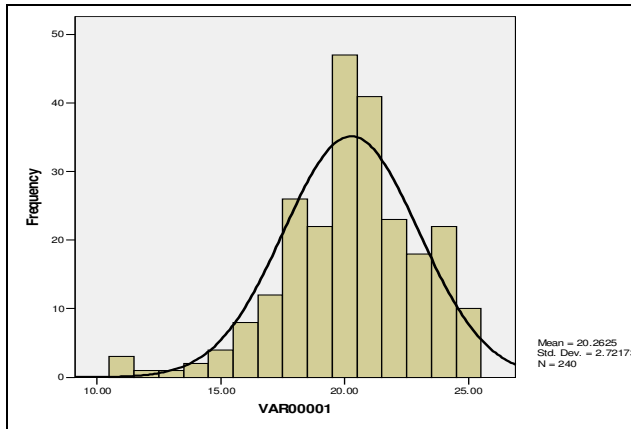
The deviation of the reiteration	minimum	maximum	average	Self-management
2.72	25	11	20.26	

The deviation of the reiteration	minimum	maximum	average	Self-management
3.29	8	25	18.13	

TABLE 3: distribution of the respondents plenty in the dimention of self-awareness.

TABLE 4: distribution of the respondents plenty in the dimension of self- management

9.2. Distribution of the Sample Plenty in the Dimension of the self-Management Rate

Based on the table 4, 62.1% of the respondents get the high grade in the rate of the self-management and 33.9% get the average grade and 4.6% get the lowest grade in this dimension by considering the grade between 5 to 25 for answering to the dimension in total, the average value that gained for the self –management is 18.1.

Comparison the Emotional Intelligence Dimensions.

Table 5 related to the comparison between the emotional effectiveness dimensions in organizations.

It is clear that, the least value and the most divergence of views pertaining to the self-awareness. Based on the variance analysis test that has done, these divergences, statistically in level is

Mehrbakhsh Nilashi, Othman bin Ibrahim, Amir Talebi & Alireza Khoshraftar

meaningful about 5%. Figure 2, shows the comparison between the emotional intelligence dimensions.

Criterion deviation	average	
2.72	20.26	Self- awareness
3.29	18.13	Self- management
2.93	19.01	Motivation
2.87	19.74	Sympathy
2.73	20.13	Social skills

TABLE 5: Comparison the average and creation deviation of the emotional intelligence samples
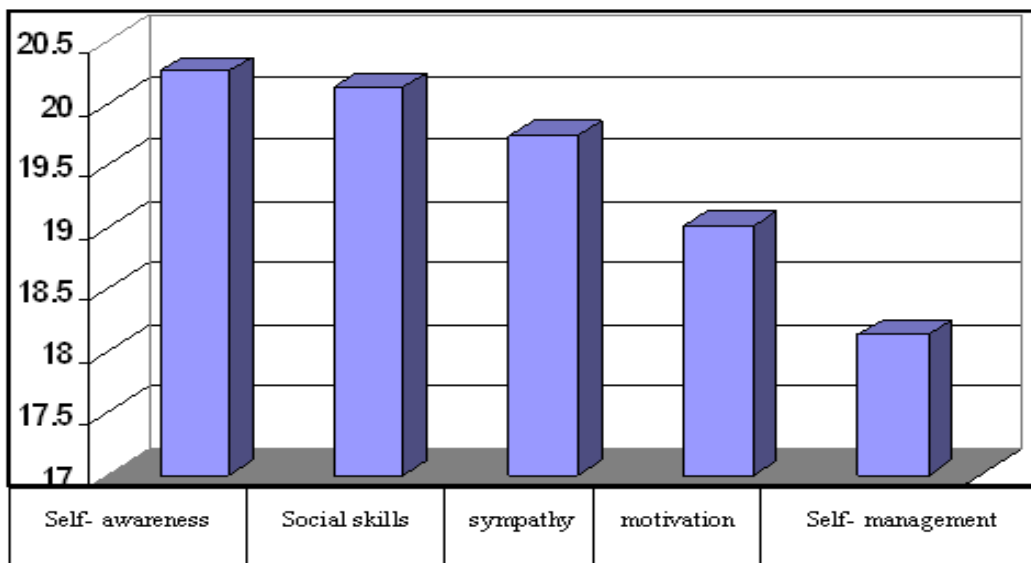
FIGURE 2: comparision between the emotional intelligence dimensions

9.3. Survey the Organizational Effectiveness

Based on the plenty distribution of answering to the questions of the organizational effectiveness questionnaire, that mentioned question" to increase the satisfaction of the client how you can change the problem in your region. "And to most disagreement is about this question "How the present prize system encourages you to work better".

To survey the answers in questions related to affective intelligence, the average and the criterion deviation have been calculated. For doing calculation, they gave the number between 1 to 5 the answer.

The most average is for the question "to increase the satisfaction of the client how you can change the problem in your region" and the least value is for the question "How the present prize system encourages you to work better."

The most view agreement relates to this question "How much time your region staff spend to answering the client questions "and" How much is your region Client's satisfaction ". And the least view agreement encourages you to work better. "

Also, 32% of the respondents get the high grade in organizational effectiveness and 64% get the average grade and only 5% get the low grade. By considering the grade between 17 to 85 for answering to this dimension, in total, the gained average value of the organizational effectiveness is 55.74.

The amount of the probability	The amount of F	Average deviation	Free rate	The total squares	source
0.0.0	21.21	19.87	24.00	476.86	**Between the groups**
		0.94	5,933.00	5,558.89	**Inside the groups**
			5957	6035.746	**Total**

TABLE 6: the variance analysis of the questions in emotional intelligence questionarie

10. STATISTICAL UNDERSTANDINGS

10.1. Main Hypothesis

The main hypothesis of this research is that, there is a relation between the organizational effectiveness and the emotional intelligence. To survey this hypothesis, we measure the grade of the organizational effectiveness and the emotional intelligence, by using the Lykert evaluation's opinion measure. They used 17 questions for calculate the organizational effectiveness grade and used 25 questions for calculate the emotional intelligence grade in questionnaire.

In fact, we can show this hypothesis statistically by using the correlation test:

The answer to the research hypothesis is negative	$H_{\circ} : \rho = 0$
The answer to the research hypothesis is positive	$H_1 : \rho \neq 0$

In other word:

There is no relation between organizational effectiveness and the emotional intelligence.	$H_{\circ}$
There is a relation between organizational effectiveness and the emotional intelligence	H_1

Imagine that the grade of the emotional intelligence and the organizational effectiveness are less, we can use the Pierson's correlation ratio test for find the linear relation as the table 7, Pierson's correlation ratio gained in relation to emotional intelligence:

Emotional intelligence	
Pierson's correlation ration	0.3282
The amount of probability	0.000

TABLE 7: the variance analysis of the questions in emotional intelligence questionnaire

10.2. Pierson's Correlation Relation to Emotional Intelligence

As showed in the table, the correlation rate between the effectiveness and emotional intelligence is 0.3282. The linear regression between the emotional intelligence and organizational effectiveness showed in figure 3.
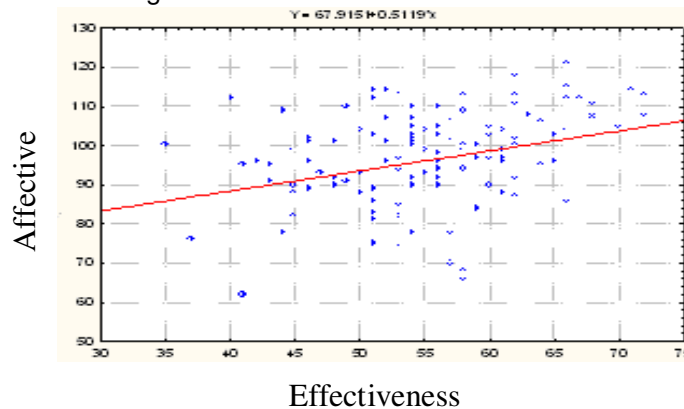
FIGURE 2: the linear regression between the emotional intelligence and organizational effectiveness.

By attention to the amount of the probability and the test level, we can say that, zero hypotheses or this hypothesis that "there is no relation between the effectiveness and emotional intelligence in organization", rejected from the 5% level and we can strongly say that, there is a relation between the organizational effectiveness and the emotional intelligence.

11. CONCLUSION

Statistical test was done over 240 managers, assistants, leader and the elders' staff of the 3 parts regions in Rasht. It showed that, there is a meaningful relation between the manager's emotional intelligence and the organizational effectiveness. by this out comes we can get the most important results from the emotional intelligence questionnaire and from the effectiveness questionnaire.

The brief outcomes of the emotional intelligence questionnaire are:

- The most average is for this question: "I have an ability to make an intimate relation with others."
- The least average is for this question: "When I want to do some thing that I don't like, I create a motivation for doing it.
- The most view agreement is for this question: "I'm aware of my internal position change."
- The least view agreement is for the question: "for changing my affective position, I talk to my self."
- 1.87% of the respondents have the high rate of self – awareness.
- 1.62% of the respondents have the high rate of self-management.
- 2.68% of the respondents have the high rate of motivation.
- 80.0% of the respondents have the high rate of sympathy.
- 4.85% of the respondents have the high rate of social skills.
- The least average and the most divergence of view are about self-awareness component.

The brief out comes of the organizational effectiveness questionnaire is:

- The most agreement was about this question: "to increase the satisfaction of the client, how you change your region problem."
- The most disagreement was about this question: "How the present prize system encourages you to work better."
- The most view agreement is mentioned for this question:" How much time you region staff spend to answer to the client.
- The least view divergence was about this question:" How the present prize system encourages you to work better."
- The gained average of the total effectiveness is 55/74. That is over the average.
- The gained outcomes from the research hypothesis test:
- The outcomes of the main hypothesis (the positive and linear relation exist between the people's emotional intelligence and the organizational effectiveness):" We can increase the organizational effectiveness by forting and training the emotional intelligence dimensions in staff.
- The obtained outcomes from the first minor hypothesis (There is a meaning relation between the staff – awareness component and the organizational effectiveness): "show the individual quality of the staff, caused the improvement of the organizational effectiveness for them.
- The obtained outcomes from the second minor hypothesis (there is a manful relation between the staff self- management component and the organizational effectiveness. "For achieving the organizational effectiveness, we need to increase the quality of the managers in order to control and management the stress."
- The obtained out comes from the third minor hypothesis (there is a meaningful relation between the staff motivation component and the organizational effectiveness): "Don't pay attention to the staff welfare caused to decline the organizational effectiveness."
- The obtained outcomes from the forth minor hypothesis (there is a meaningful relation between the staff sympathy component and the organizational effectiveness): "the organizational effectiveness increased, if the managers have a good relationship with their staff.
- The obtained outcomes from the fifth minor hypothesis (there is a meaningful relation between the social skills components and the organizational effectiveness): "Managers need to create a management network within the staff's relation in order to achieve the goals and determine the responsibilities.

12. RECOMMENDATION

A suggestion to the organizations managers:

- Rein force the emotional intelligence of the staff by training.
- Pay attention to the emotional intelligence as a selection criterion, when selecting the new staff.
- Measure the emotional intelligence rate of the staff, in period and recognize the week component.
- Review the responsibilities and the powers for the managers that gained the lowest value in self-management component.
- Review the staff's welfare for the managers that gained the low value in motivation component.
- Suggestion for other researchers:
- In this research, the relation between effectiveness and emotional intelligence was evaluated and we can evaluate this relation with the groups' emotional intelligence.
- New out look in emotional intelligence was planned within the organization, as, "the emotional intelligence of organization 1 that we can substitute the emotional intelligence component by its components. The components of this emotional intelligence described as follow:
- The organizational self-awareness : knowing the week and power points in an organization, be aware of the emotional currents that present in an organization and use that awareness , for creating a good company that is known by trust , reliable .
- The organizational self-management: survey and manage the organizational emotional in order to help the organization not to hurt it ; the organizations that are intelligence emotionally survey the present emotional currents in order to find the negative method and recognize them.
- The organizational culture, that caused the staff work in best way and provide a chance to improve their qualities and use them in order to improve their position in an organization.
- Sympathy: know and understand the requirement, emotional and worries of the organizations internal and external share holders.
- The organizational social skills: manage the organizational relation by creating and holding the relation within the internal and external share holders.

13. References

[1]   Wilson, W. (2008) 'Emotional Intelligence & Organizational Effectiveness', Psychology Hatrold Abel School of Psychology Capella University.

[2]   Ostroff, C.; Schmitt, N (1993) 'Configurations of Organizational Effectiveness and Efficiency', Academy of management Journal 36: 1345 – 61.

[3]   Goleman, D., (1998) 'Emotional Intelligence– Why it can matter more than IQ'.

[4]   Bar-On, R. (1997). Emotional Quotient Inventory: Technical manual. Toronto: Multi-Health Systems.

[5]   Armstrong, m. (2001).'Hand book of human resource management praetice', 8 the editions, USA. Kogan pag.

[6]   L. Angley, A. (2000). Emotional intelligence a new realization for management development? Career Development international5 (3), 177 –183A. Author 1 and B. Author 2, "Title of the journal paper" IEEE Trans. Antennas and Propagation, Vol. 55, No. 1, pp. 12-23, and 2007.

[7]   Palmer, B. R., & Stough, C. (2007). A confirmatory factor analytic investigation of the TAS-20: Corroboration of a five-factor model and suggestions for improvement. Journal of Personality Assessment, 89, 247-

[8]   Abraham, R. (2004). Emotional competence as antecedent to performance: A contingency framework. Genetic Social and General Psychology Monographs, 130(2), 117-145.

[9]   Bliss's. (2002) 'The Affect of Emotional Intelligence on a Modern Organization Leader's Ability to Make Effective Deasion', Bellevus University.

[10]   Mayer, J. Rabits, R., (2008) 'The scope of Emotional Intelligence', Annual Rev – Psychology.

Enaiyat Ghani Ovy, H.A.Chowdhury, S.M.Ferdous, Shakil Seeraji & Kazy Fayeen Shariar

A Novel Approach Concerning Wind Power Enhancement

Enaiyat Ghani Ovy   *enaiyat_ovy@yahoo.com*
Department of Mechanical & Chemical Engineering
Islamic University of Technology
Board Bazar, Gazipur-1704, BANGLADESH

H.A.Chowdhury   *Chowdhh2@mail.dcu.ie*
Department of Mechanical & Chemical Engineering
Islamic University of Technology
Board Bazar, Gazipur-1704, BANGLADESH

S.M.Ferdous   *tanzir68@gmail.com*
Department of Electrical & Electronic Engineering
Islamic University of Technology
Board Bazar, Gazipur-1704, BANGLADESH

Shakil Seeraji   *shakil.ae@mist.edu.bd*
Department of Aeronautical Engineering
Military Institute of Science and Technology
Mirpur Cantonment, Dhaka-1216, Bangladesh

Kazy Fayeen Shariar   *eshankonerbaiu@yahoo.com*
Department of Electrical & Electronic Engineering
Islamic University of Technology
Board Bazar, Gazipur-1704, BANGLADESH

Abstract

Being a tropical country, Bangladesh does have wind flow throughout the year. However, the prospect for wind energy in Bangladesh is not at satisfactory level due to low average wind velocities at different regions of the country. The field survey data indicated that the wind velocities are relatively higher from the month of May to August, whereas, it is not so for the rest of the year. Therefore, exploiting the wind energy at low wind velocities is a major predicament in creating a sustainable energy resource for a country with inauspicious forthcoming energy crisis. The scope of this paper concentrates on an innovative approach to harness wind power by installing an auxiliary unit which would only assist the primary turbine unit in case the wind velocity falls under the required value. The auxiliary unit would comprise a secondary turbine, which would be operated by a DC motor connected to a battery system that is charged by a solar panel. A specially designed conduit would encompass both the primary and auxiliary turbine units. A CFD simulation utilizing ANSYS FLOTRAN was carried out to investigate the velocity profiles for different pressure differences at different regions of the prototype conduit. A feasibility analysis of the modified system was eventually carried out for the preferred conduit design.

Keywords: Wind Energy, Solar Energy, CFD, FEM, Wind Power Enhancement.

1. INTRODUCTION

It is well known that the main drawback of wind power is the inherent variable behavior. Significant research has been carried out to improve the performance of the wind turbines to enhance the performance and establish the power system stability. Novel and significant designs of the wind turbines were developed during last few years. From the scientific literature survey it was found that a wind turbine system was developed which consists of a diffuser shroud with a broad-ring flange at the exit periphery and a wind turbine inside it for obtaining a higher power

output [1]. Also for the optimization of the wind turbine energy as well as power factor an evolutionary computation algorithm was established. This evolutionary strategy algorithm solves the data-derived optimization model and also determines optimal control settings for the wind turbine [2]. To obtain a reliable and steady output of power, wind turbines are generally integrated with conventional solar panel or biomass energy or hydro power systems. From the previous research works hybrid photovoltaic wind energy system was analyzed to provide better electricity output to the grid [3]. From the literature survey it was also found that the Hybrid Solar-Wind System Optimization Sizing (HSWSO) model was developed to optimize the capacity sizes of different components of hybrid solar-wind power generation systems that employ a battery bank. A case study was reported in that paper to show the importance of the HSWSO model for sizing the capacities of wind turbines, PV panel and battery banks of a hybrid solar-wind renewable energy system [4]. Wind power was also complemented by hydropower to obtain firm power output. For getting constant power output in a hybrid power station without the intermittent fluctuations inherent when using wind power a conceptual framework was provided [5]. Wind power could be also integrated with bio energy. An innovative system combining a biomass gasification power plant, a gas storage system and stand-by generators to stabilize a generic 40 MW wind park was proposed and evaluated with real data [6]. In this current study, a novel design is proposed to enhance the wind power. A primary turbine is placed in a conduit inlet which would be governed by a secondary turbine at low wind speed placed in the conduit outlet. The secondary turbine would be coupled with a DC motor where the motor would be directly connected to the battery bank. The battery would be charged by the solar panel. This design mainly encompasses the scenario where the wind speed fluctuates in a significant manner. For example, the prospect for wind energy in Bangladesh is not at satisfactory level due to low average wind velocities at different regions of the country. However, there are some places in Bangladesh like coastal areas where wind speed is relatively higher for harnessing power but is not constant for all the time during power extraction. So the primary concentration would be to extract power at relatively low wind speed. In this paper, an innovative approach is shown with clear description to enhance the wind power and simulation of the design is also provided. Finally a comparative feasibility analysis of the modified system with the conventional wind turbine is given with elaborate mathematical explanations.

The following table gives information about the monthly variation of wind speed in some places of Bangladesh. It is clear that the wind speed is not constant for power extraction at promising level during a certain year, rather, it fluctuates in a significant manner. It shows that during few months for certain regions in the country power extraction from the wind turbine is not at all possible.

Locations	Months												
	Jan	Feb	Mar	Apr	May	Jun	Jul	Aug	Sept	Oct	Nov	Dec	Mean
Barisal	2.90	2.57	2.57	3.56	3.23	2.90	2.71	2.64	2.57	2.11	2.07	2.05	2.66
Bogra	1.95	2.20	3.05	4.03	4.15	3.66	3.42	3.05	2.56	2.20	1.83	1.71	2.82
Chittagong	3.64	2.88	4.95	5.01	5.51	6.89	7.09	6.83	4.64	2.82	3.39	2.20	4.65
Comilla	2.26	2.70	2.57	5.45	3.83	3.20	2.88	2.95	1.82	2.38	1.63	1.70	2.78
Cox'sBazar	3.76	3.83	4.51	5.58	3.83	4.14	3.83	3.95	3.20	3.26	2.57	3.26	3.81
Dhaka	3.39	3.26	4.39	5.77	6.33	5.71	6.01	5.89	4.39	3.45	2.64	2.95	4.52
Dinajpur	2.68	2.44	4.88	2.44	2.93	2.68	2.56	2.44	2.44	3.54	2.44	2.44	2.83
Hatiya	3.04	2.64	4.16	3.97	4.82	6.47	5.75	2.64	2.96	2.77	3.06	2.57	3.74
Jessore	2.88	2.95	4.95	8.34	8.34	6.27	6.15	4.95	4.33	3.45	3.32	3.20	4.93
Khepupara	4.20	4.39	3.83	7.09	5.83	4.71	4.14	3.95	3.57	3.70	2.95	2.57	4.24
Khulna	2.96	1.65	3.04	3.05	4.16	3.89	3.31	2.44	2.51	1.98	3.31	2.38	2.89
Kutubdia	1.77	1.82	2.32	2.70	2.77	3.65	3.61	3.14	2.11	1.45	1.19	1.29	2.32
Mongla	1.07	1.25	1.72	2.51	2.92	2.63	2.48	2.35	1.83	1.27	1.02	1.01	2.20
Rangamati	1.45	1.65	4.42	3.10	2.11	3.23	1.72	2.24	1.45	1.45	1.39	1.59	2.15
Sandip	2.32	3.01	3.20	4.83	2.44	3.83	3.39	2.70	2.32	1.63	1.70	1.70	2.76
Sylhet	2.20	2.93	3.29	3.17	2.44	2.68	2.44	2.07	1.71	1.95	1.89	1.83	2.38
Teknaf	3.70	4.01	4.39	4.01	3.32	3.89	3.83	2.88	2.44	2.20	1.57	1.76	3.17
Patenga	6.22	6.34	7.37	7.92	8.47	8.69	9.20	8.54	7.48	6.93	6.71	5.91	7.48
Sathkhira	4.21	4.40	3.84	7.10	6.11	4.76	4.27	4.03	3.62	3.78	3.54	2.81	4.37
Thakurgaon	4.15	5.06	7.93	8.43	8.66	8.05	7.93	6.59	6.34	5.98	5.25	4.76	6.59

TABLE 1: Average Wind Speed (m/s) at 20 Meters Height at Different Locations in Bangladesh [7].

2. Basic Theory

W. J. M. Rankine and W. E. Froude established the simple momentum theory for application in the ship's propeller. Later, A. Betz of the Institute of Gotingen used their concept to the windmill.
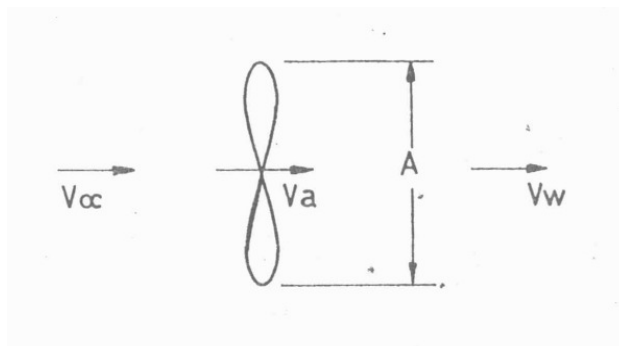
FIGURE 1: Flow velocities through a windmill.

As shown in the fig.1, the symbols, and   respectively are the free stream wind velocity, induced velocity and wake velocity. When the flow occurs through the windmill, the flow is retarded and it is further retarded in the downstream side of the windmill. The flow velocity through the windmill is usually called the induced velocity, while the flow velocity in the downstream side is called the wake velocity because wake is formed there. According to the Newton's Second law of motion the thrust developed in the axial direction of the rotor is equal to the rate of change of momentum i.e.

$$\text{Axial Thrust} = m(V_\infty - V_w)$$

(1)

Where m is the mass of air flowing through the rotor in unit time.

Therefore, the power produced is given by,

$$P = m(V_\infty - V_w)V_a$$

(2)

The rate of kinetic energy change in the wind is,

$$\Delta K.E / \sec = \frac{1}{2}m(V_\infty^2 - V_w^2)$$

(3)

Now balancing the equations (2) and (3),

$$m(V_\infty - V_w)V_a = \frac{1}{2}m(V_\infty^2 - V_w^2)$$

(4)

After simplifying the equation (4), one obtains

$$V_a = \frac{V_\infty + V_w}{2}$$

(5)

Glauert determined the identical expression in his actuator disc theory. Here the flow is assumed to occur along the axial direction of the rotor and the velocity is uniform over the swept area, A of the rotor.

Since, $m = A\rho V_a$, from the equation (2), one finds the expression of power extraction through the rotor,

$$P = \rho A V_a (V_\infty - V_w) V_a \tag{6}$$

Where, ρ is the density of air. Substituting the value of V_a from the equation (5) in the equation (6),

$$P = \rho A V_a^2 (V_\infty - V_w) = \rho A (\frac{V_\infty + V_w}{2})^2 (V_\infty - V_w)$$

which can be rewritten as,

$$P = \frac{\rho A V_\infty^3}{4}(1 + \frac{V_w}{V_\infty})[1 - (\frac{V_w}{V_\infty})^2] \tag{7}$$

Inserting $x = \dfrac{V_w}{V_\infty}$ in the equation (7),

$$P = \frac{\rho A V_\infty^3}{4}(1 + x)(1 - x^2) \tag{8}$$

Now differentiating P of the equation (8) with respect to x and setting it to zero for maximum power, one obtains,

$$x = \frac{V_w}{V_\infty} = \frac{1}{3} \tag{9}$$

Substituting $V_w = \dfrac{V_\infty}{3}$ in the equation (7) and simplifying, the expression of maximum power extraction is obtained as,

$$P_{\max} = \frac{8}{27}\rho A V_\infty^3 \tag{10}$$

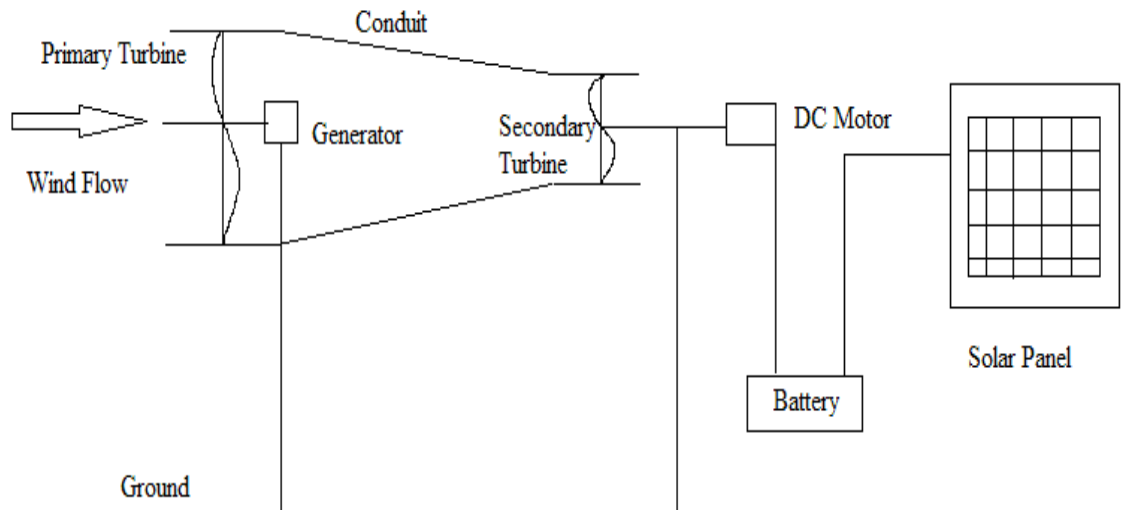The available energy in the wind is the kinetic energy per unit time,

$$K.E/_{\sec} = \frac{1}{2}m_i V_\infty^2 = \frac{1}{2}\rho A V_\infty^3 \tag{11}$$

Here mass of air (m_i) flowing through the rotor has been considered to be ideal i.e. full air flows through the rotor, as such $m_i = A\rho V_\infty$.

## 3. Modification and Design for Wind Power Enhancement

FIGURE 2: Schematic of the proposed modified design of the system.

As shown in fig.2, the primary turbine and the secondary turbine would be set at the inlet and the outlet of the taper shaped conduit consecutively. The primary turbine would comprise a generator which would be installed inside the conduit. The secondary turbine would run by a DC motor which would be connected to the battery system that would be charged by the solar panel. A PV solar panel would be used as a back up source for the DC motor.

When the wind speed would reach the desired level for power extraction the primary turbine would start to rotate and would give a certain power output. The wind would then pass through the conduit striking the blades of the auxiliary turbine with a relatively low energy compared with the inlet wind energy. The converging section of the conduit is helpful in increasing the air velocity that could be utilized to run the auxiliary unit effectively. Therefore power would also be produced by the auxiliary unit where the DC motor will act as a generator. Next when the wind speed goes down below the desired level then the secondary turbine will run with the help of DC motor to assist the primary turbine to rotate. In this case the primary turbine delivers the electrical power whereas the secondary unit gets the power from the DC motor connected to the battery bank. When the wind speed again reaches at the desired level then the DC motor will stop and act as a generator because of the natural wind flow through the secondary turbine. The overall power extraction as well as system efficiency is enhanced with the help of this proposed design. In the next two sections the feasibility of this proposed system is justified with simulation and mathematical calculations.

4. SIMULATION RESULTS

ANSYS FLOTRAN simulations were carried out with steady state, standard κ-ε turbulent model for varying downstream diameters of the conduit with varying pressure differences. From the simulations results depicted in fig.3, downstream diameter of 0.6 meter with upstream and downstream pressure difference of 30 Pa was selected to be the preferred parameters as this would provide the cut-in velocity of 5 m/s in the upstream region of the conduit. Fig.4 depicts the air velocity profile with the selected parameters.
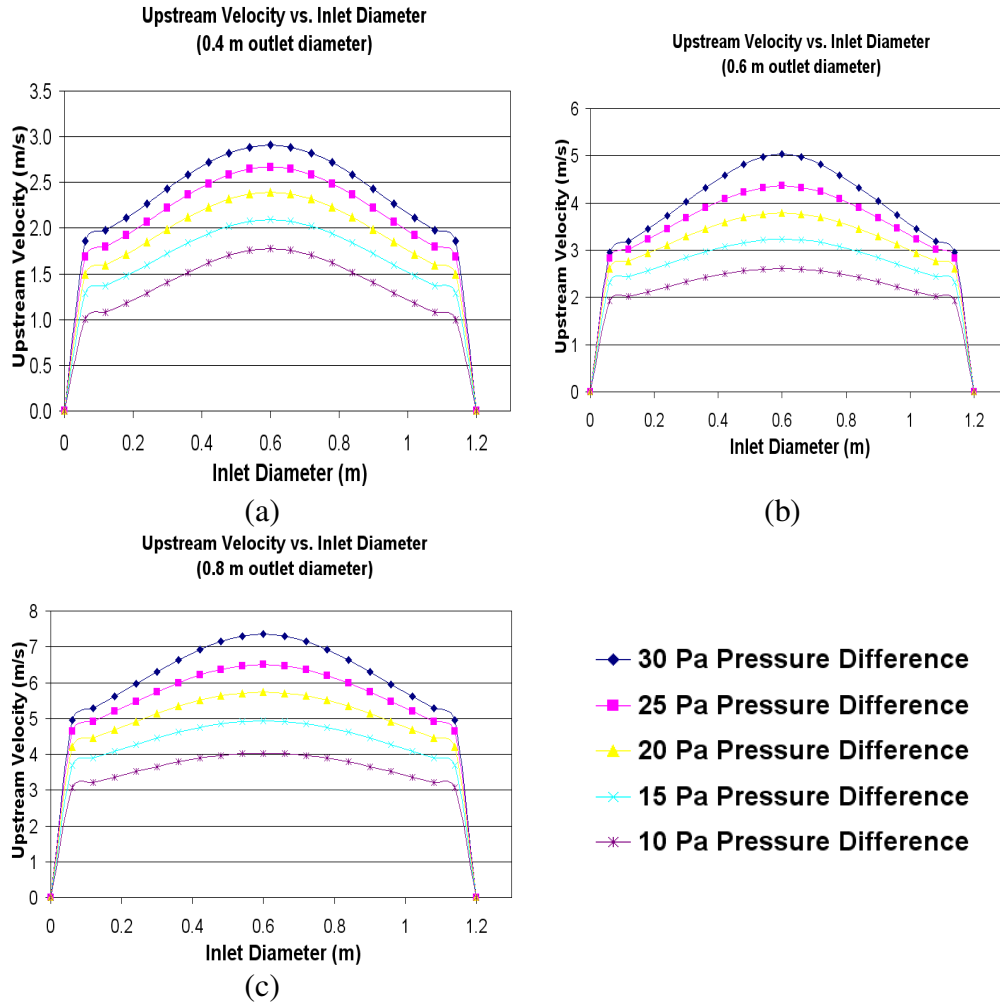
FIGURE 3: Upstream velocity vs. inlet diameter of the conduit for the outlet diameter of (a) 0.4m, (b) 0.6m, and (c) 0.8m.
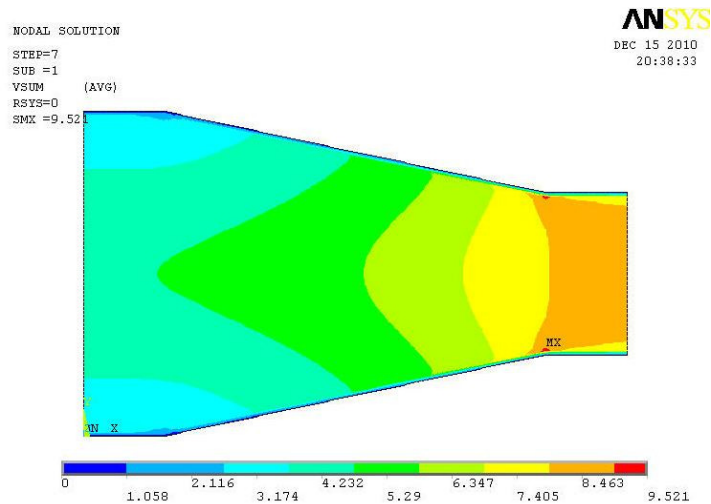
FIGURE 4: Velocity profile of air through the conduit (0.6m outlet diameter, pressure difference 30 Pa).

5. FEASIBILITY ANALYSIS OF THE MODIFIED SYSTEM
The feasibility analysis of the modified system is based on theoretical calculations. Here all conditions are assumed ideal.

Assumptions:
Diameter of the primary wind turbine = 1.1m
Diameter of the secondary wind turbine = 0.5m
Cut-in speed for 1.1m diameter turbine = 5m/s (approximated)

Inlet velocity at the primary turbine, $V_1 = 5m/s$

Inlet velocity at the secondary turbine, $V_2 = 8m/s$

The velocity variations were considered from the simulation results.

From fig.5, considering a specific scenario for the Cox's Bazar region, the theoretical calculation for feasibility analysis was carried out. From the figure it can be seen that, in the Cox's Bazar region cut-in speed could be achieved for the period of 12 hours for power extraction. However, for the remaining 12 hours, the wind speed is below the cut-in speed. Here, an analytical solution was attempted considering the cut-in speed as the maximum tolerance limit of 5 m/s.
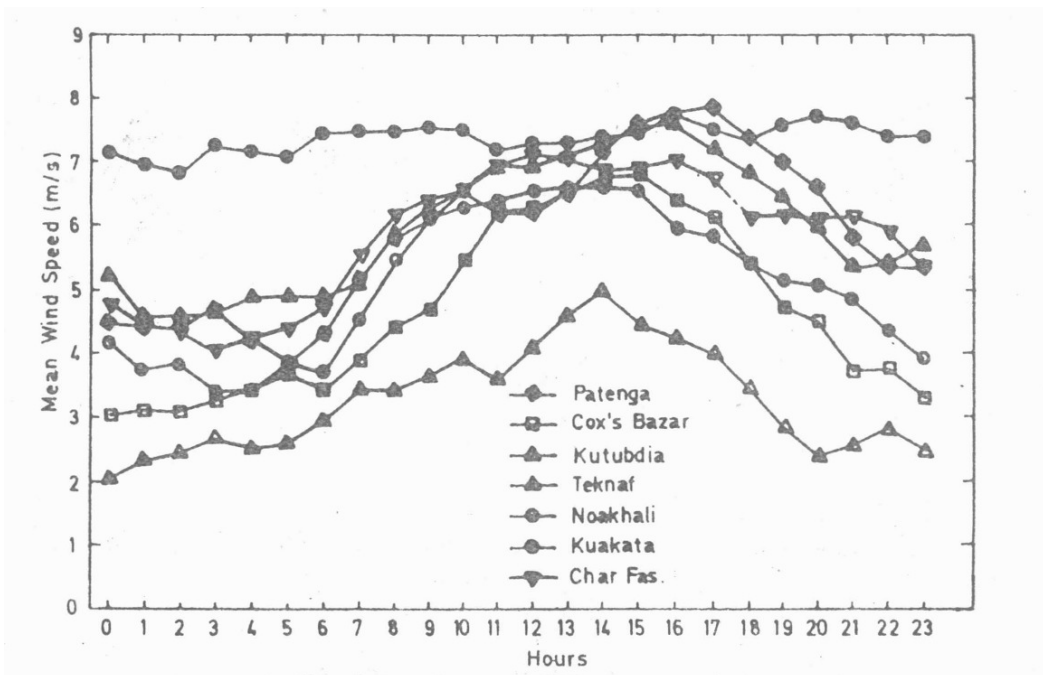

FIGURE 5: Diurnal Variation of Wind Speed in Some Places of Bangladesh [8].

For 12 hours when wind speed is at the cut-in speed of primary turbine the energy output from

the primary turbine is $E_1 = \dfrac{8}{27} \rho A V_\infty^3 \times t$ =1824.64 KJ (Considering equation 10)

And for 12 hours the energy output also from the secondary turbine is $E_2 = 1544.16 KJ$

Now for the rest of the 12 hours period when wind speed is below the cut-in speed of the primary

turbine energy output from the primary turbine is $E_3 = 1824.64 KJ$

And for 12 hours period energy input to the secondary turbine is

$$E_4 = \frac{1}{2}\rho Q(V_2^2 - V_1^2) \times t = 1587.89 KJ$$

The net energy output from the system is $E = E_1 + E_2 + E_3 - E_4 = 3605.55 KJ$

Energy output from the same conventional wind turbine which would only work for 12 hours period is theoretically, $E_5 = 1824.64 KJ$

Thus, during 24 hours, the amount of energy enhanced from the modified system was $(E - E_5) = 1780.91 KJ$ or 20.61W. Here minimum energy has been gained considering the cut-in velocity. More energy could be harnessed when the wind flows at relatively higher speeds.

6. CONCLUSION AND FUTURE WORK

In this current research work a conceptual design has been proposed which was validated by the ideal theoretical formulations. Simulation results showed the wind speed variations through the conduit. Wind power could be enhanced by a certain amount by implementing this novel design. This feasible design could be implemented where wind speed is not at satisfactory level like Bangladesh. It would be beneficial if energy of the wind can be extracted at relatively low speed. Further research is currently being held regarding the prototype manufacturing and testing. Subsequently, the economical viability of the overall system would also be analyzed.

7. REFERENCES

[1] Yuji Ohya, Takashi Karasudani, Akira Sakurai, Ken-ichi Abe, Masahiro Inoue, Development of a shrouded wind turbine with a flanged diffuser, Journal of Wind Engineering and Industrial Aerodynamics, Volume 96, Issue 5, May 2008, Pages 524-539.

[2] Andrew Kusiak, Haiyang Zheng, Optimization of wind turbine energy and power factor with an evolutionary computation algorithm, Energy, Volume 35, Issue 3, March 2010, Pages 1324-1332.

[3] N. B. Urli, M. Kamenski, Hybrid photovoltaic/wind grid-connected power plants in Croatian renewable energy program, Renewable Energy, Volume 15, Issues 1-4, September-December 1998, Pages 594-597.

[4] Hongxing Yang, Lin Lu, Wei Zhou, A novel optimization sizing model for hybrid solar-wind power generation system, Solar Energy, Volume 81, Issue 1, January 2007, Pages 76-84.

[5] O. A. Jaramillo, M. A. Borja, J. M. Huacuz, Using hydropower to complement wind energy: a hybrid system to provide firm power, Renewable Energy, Volume 29, Issue 11, September 2004, Pages 1887-1909.

[6] A. Pérez-Navarro, D. Alfonso, C. Álvarez, F. Ibáñez, C. Sánchez, I. Segur, Hybrid biomass-wind power plant for reliable energy generation, Renewable Energy, Volume 35, Issue 7, July 2010, Pages 1436-1443.

[7] Sultan Ahmmed and M. Quamrul Islam, Wind Power for Rural Areas of Bangladesh, 3rd International Conference on Electrical & Computer Engineering, ICECE 2004, Pages 192-197, 28-30 December 2004, Dhaka, Bangladesh.

[8] A. C. Mandal, M. Q. Islam, Aerodynamics and Design of Wind Turbines, ISBN 984-31-0923-0, September 15, 2001, Published by BUET, Dhaka-1000.

Satellite-and Ground-Based Red Tide Detection Method and System by Means of Peak Shift of Remote Sensing Reflectance

Kohei Arai   *arai@is.saga-u.ac.jp*
Information Science Department
Saga University
Saga City, 840-8502, Japan

Yasunori Terayama   *terra@is.saga-u.ac.jp*
Information Science Department
Saga University
Saga City, 840-8502, Japan

Abstract

A method for detection of red tide by means of remote sensing reflectance peak shift is proposed together with suspended solid influence eliminations. Although remote sensing reflectance peak is situated at around 550nm for sea water without suffered from red tide, the peak is shifted to the longer wavelength when sea water is suffered from red tide. Based on this fact, it is capable to detect red tide using high wavelength resolution of spectroradiometers. The proposed system uses green color filtered cameras. Acquired imagery data can be transmitted through wireless LAN to Internet terminal and can be archived in server through Internet. This is the proposed ground based red tide monitoring system. The paper also proposes a method for removing suspended solid influence on red tide suffered area estimations. The proposed method and system is validated in laboratory and field experiments. The system is deployed at coastal areas of the Ariake Sea in Kyushu, Japan.

Keywords: Red Tide, Remote Sensing Reflectance, MODIS, Sensor Network.

1. INTRODUCTION

In accordance with increasing of phytoplankton concentration, sea surface color changes from blue to green as well as to red or brown depending on the majority of phytoplankton (Dierssen et al, 2006) so that it is capable to detect red tide using this color changes [1]. It is also possible to detect red tide using Moderate Resolution Imaging Spectroradiometer: MODIS ocean color bands data. Almost more than 90 % of reflected radiance in the visible to near infrared wavelength region from the ocean is derived from the atmosphere so that atmospheric correction is needed before red tide detection. An iterative approach (Arnone et al., 1998 [2]; Stumpf et al., 2003 [3]) for sediment-rich waters, based on the Gordon and Wang (1994) algorithm [4], is used to correct for the atmospheric interference in the six ocean color bands of MODIS in turbid coastal waters to obtain water leaving radiance, which are then used in the band-ratio algorithm (O'Reilly et al., 2000 [5]) to estimate Chlorophyll in unit of mg m^{-3}. Also suspended solid is estimated with two bands algorithm (visible minus near infrared bands data). The multi-channels of red tide detection algorithms (in the formula of $C=(R_i-R_j)/(R_k-R_l)$ where R_i, R_j, R_k and R_l are the reflectivity derived from bands *i, j, k* and *l*.) are proposed. Also learning approaches based on k-nearest neighbors, random forests and support vector machines have been proposed for red tide detection with MODIS satellite images (Weijian C.,et al.,2009) [6].

One of the problems on the conventional satellite imagery data based red tide detection methods is that detection accuracy is not good enough followed by elimination of influence due to suspended solid from the detected red tide. The procedure of the proposed method is to estimate red tide index C together with suspended solid first, then remove the influence due to suspended solid from the estimated red tide index by comparing both. Atmospheric correction is out of scope

of the paper because there are atmospheric corrected MODIS data products. The proposed method is based on the multi-channels of red tide detecting algorithm with suspended solid influence eliminations.

The paper also proposes ground based red tide monitoring system. The system uses camera data with green color filter. Red tide contaminated sea water shows remote sensing reflectance wavelength peak shift so that camera data with green color filter of red tide contaminated sea are shows a little bit higher radiance rather than that of just sea water without contamination. Acquired camera data is transmitted through wireless LAN (local Area Network) and Internet. This is a ground based measurement system which allows red tide detection even in the cloudy and rainy weather conditions; satellite imagery data based method does not work in such weather conditions.

The following section describes the proposed method followed by some experimental results. The final section describes conclusions and some discussions.

2. THE PROPOSED RED TIDE DETECTION METHOD AND SYSTEM

2.1   Method for Red Tide Detection With MODIS Data

The multiband ratio algorithms for red tide detection is expressed as follows,

$$C = (R_i - R_j)/(R_k - R_l) \qquad\qquad (1)$$

where R_i, R_j, R_k and R_l are the reflectivity derived from bands i, j, k and l. If $C \geq t$, then the pixel is assumed to be red tide suffered, where t is a threshold. It is expressed with MODIS bands 8, 10, and 12 (See Table 1) as follows,

$$C = (R_8 - R_{10})/(R_{12} - R_{10}) \qquad\qquad (2)$$

MODIS Band 8	405 – 420nm	Radiance 44.9	S/N ratio 880
9	438 - 448	41.9	838
10	483 - 493	32.1	802
11	526 - 536	27.9	754
12	546 - 556	21.0	750
13	662 - 672	9.5	910
14	673 - 683	8.7	1087
15	743 - 753	10.2	586
16	862 - 877	6.2	516

TABLE 1: Wavelength coverage of MODIS (Ocean channels)

Chlorophyll, pigments, fatty acids, total suspended solids, sediments, and Color Dissolved Organic Matter: CDOM absorption is closely related each other. In particular, it is used to occur red tide is detected together with suspended solids. Suspended solids influence on red tide detection has to be eliminated from the calculation of C. Suspended solid can be expressed as follows,

$$ln(S)=VIS-NIR \tag{3}$$

where *VIS* and *NIR* denotes visible band data and near infrared band data, respectively. MODIS bands 9 and 16 are selected for visible and near infrared channels of data, respectively. Absorption coefficients at the wavelength of 440nm is proportional to *S* so that *S* can be calculated with MODIS band 9 data, M_9 based on the following equation,

$$S=C_1-C_2M_9 \tag{4}$$

where *Ci* is regressive coefficients. *Ci* can be determined through a regression analysis. Also, equation (5) is used for the regression analysis.

$$ln(C_1)=C_0(M_9-M_{16})ln(C_2M_9) \tag{5}$$

Then detected red tide pattern is compared to the suspended solid pattern for compensation of suspended solid influences on red tide detections.

2.2 Red Tide Monitoring System With Camera Data With Green Color Filter

Figure 1 shows the proposed red tide monitoring system with the band-pass filter (@550nm) attached web camera together with water quality measuring instruments as well as meteorological data collection robot.
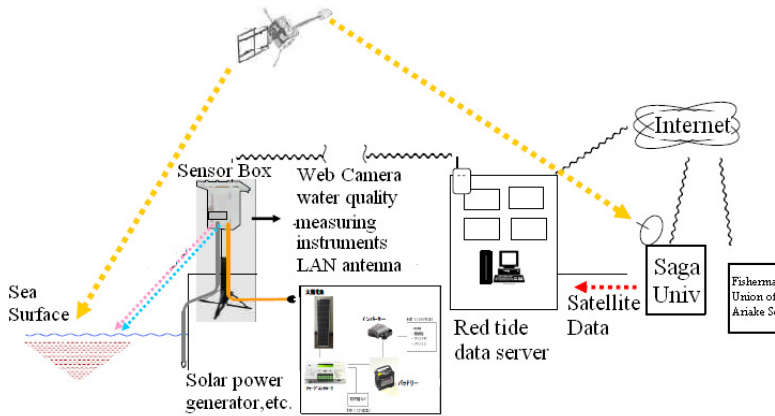
FIGURE 1: The proposed red tide monitoring system with the band-pass filter attached web camera together with water quality measuring instruments as well as meteorological data collection robot

Due to the fact that remote sensing reflectance peak is shifted to longer wavelength than 550nm for red tide suffered sea water, the band-pass filtered (550nm) camera data might be possible to indicate existence of red tide. Figure 2 shows a set of example of the spectral reflectance of normal and red tide contaminated sea surfaces.
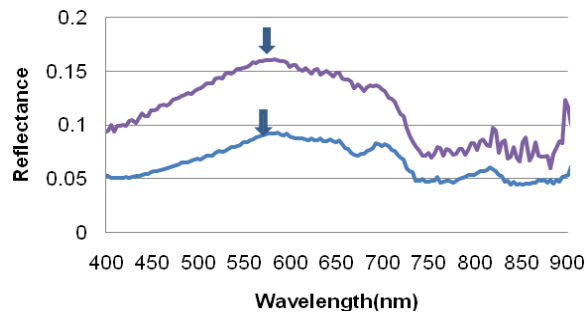
FIGURE 2: Sea surface reflectance measured at the Nanaura in Kyushu, Japan on April 20 (top: normal condition) and August 10 (bottom: red tide contaminated) 2010

The peak spectrum of red tide contaminated sea surface (August 10) is a little bit longer than that of normal condition of sea surface (April 20). Therefore, it is possible to detect red tide using green filtered camera imagery data.

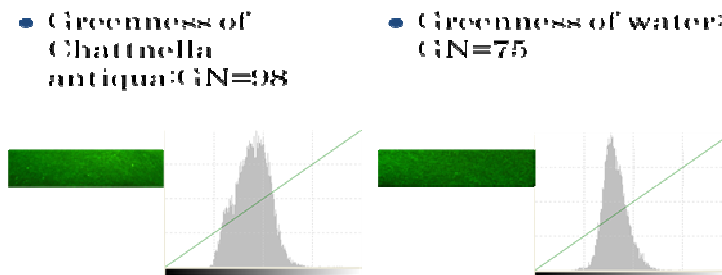## 3. EXPERIMENTS

3.1 Camera data with green color filter

Camera data with green color filter of Chattonella Antiqua containing water and just water are acquired together with histograms. The results are shown in Figure 3 and 4, respectively.
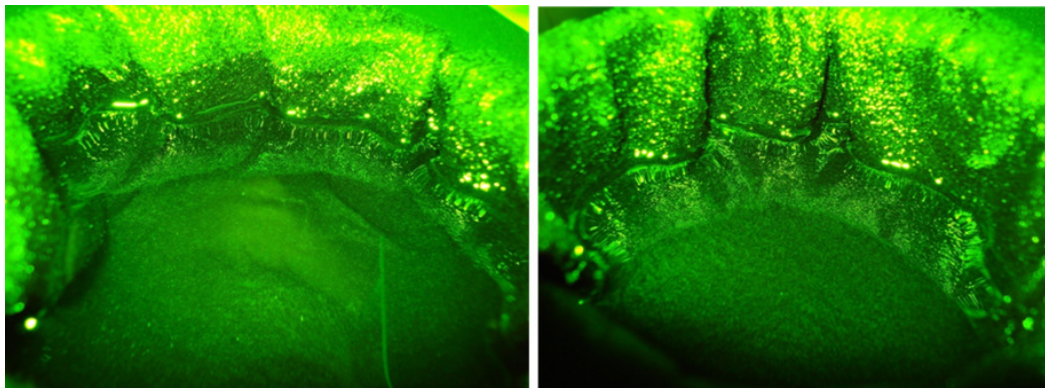
(a) Chattonella Antiqua containing water   **(b) Just water**

FIGURE 3: Camera data with green color filter of Chattenella Antiqua containing water and just water

FIGURE 4: Histogram of the camera data with green color filter of Chattonella Antiqua containing water and just water

Also camera data with green color filter are acquired in the field at the Nanaura coast in the Ariake Sea, Kyushu, Japan on the different days. Figure 5 and 6 shows the results. There are so many red tide events in the period as follows,
May 21: Heterosigma:10, Skeletonema spp.:7125
June 25: Heterosigma:100, Skeletonema spp.:6450→G=160
July 5: Chattonella Antiqua:480, Chattonella spp.:130
July 20: Skeletonema spp.:88000→G=175
August 2: Cript: 18000
August 10: Chattonella Antiqua:1080→G=140
August 17: Thalassiora spp.:6000, Skeletonema spp.:7250, Chattonella spp.:1400→G=120
November 22: Akasiwo sanguinea: 640→G=125

The number after the name of red tide type denotes the number of counted red tide while G denotes the average of the camera data with green color filter. Both the insitu data of the number of red tide provided by the Saga Prefectural Ariake Fishery Promotion Center: SPAFPC and the average of camera data with green color filter show a good correlation and coincidence.

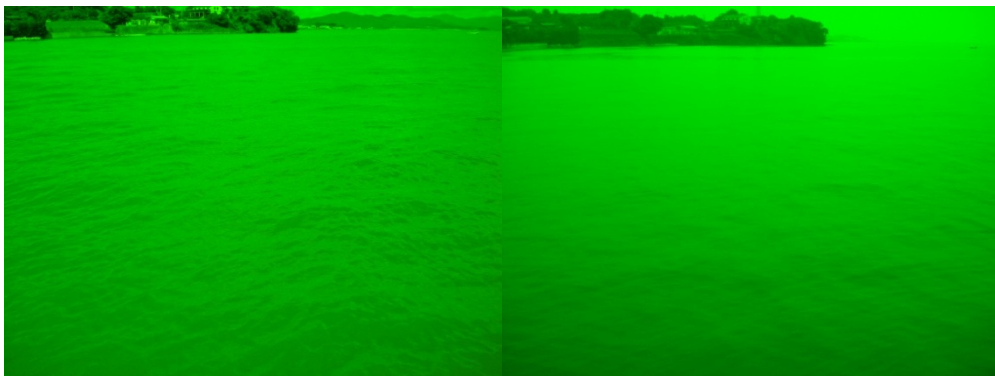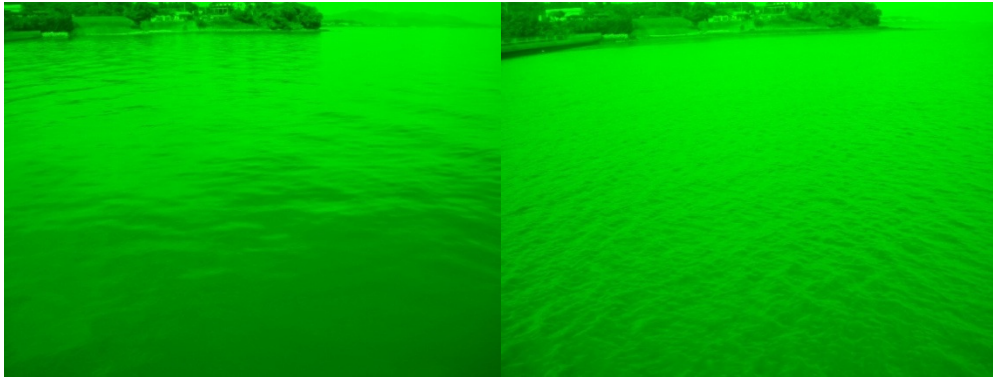**(a) June 23**   **(b) July 25**
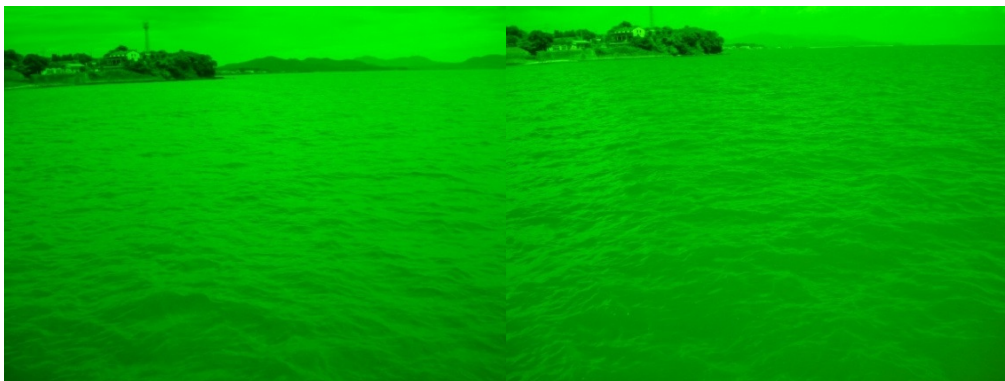
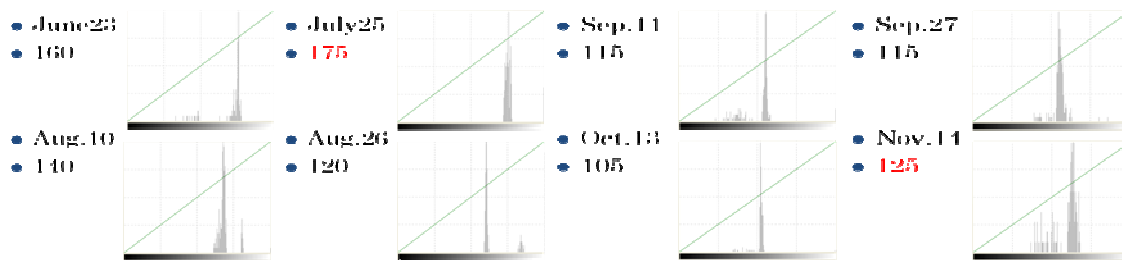**(c) August 10**   **(d) August 26**

(e) September 11   **(f) September 27**

**(g) October 23**　　　　　　　　　　**(h) November 14**

FIGURE 5: Camera data with green color filter of the Nanaura sea surface at the Ariake Sea in Kyushu, Japan on the different days in 2010.

FIGURE 6: Histograms of the acquired camera data with green color filter of the different days.

3.2　MODIS Based Red Tide Index, C

Figure 7 shows MODIS based red tide index C together with red tide events provided by SPAFPC.
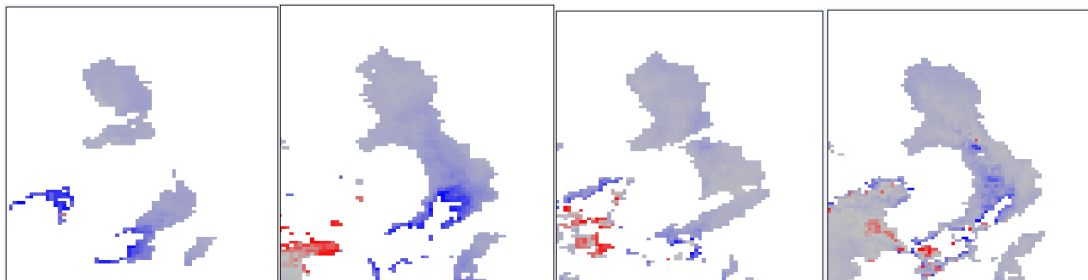
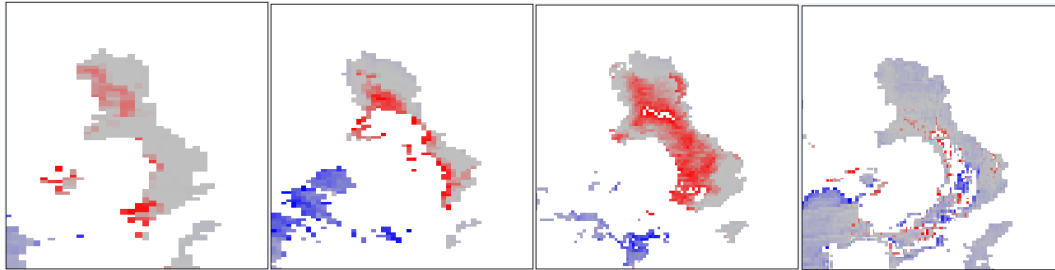**(a) 2010/05/1**　　　　**(b) 2010/05/17**　　　　**(c) 2010/06/02**　　　　**(d) 2010/06/09**
May 21: Heterosigma:10 Skeletonema spp.:7125,
June 25: Heterosigma:100, Skeletonema spp.:6450,
July 5: Chattonella Antiqua:480, Chattonella spp.:130, July 20: Skeletonema spp.:88000

(e) 2010/07/20   (f) 2010/08/06   (g) 2010/08/18   (h) 2010/11/20
August 2: Cript:18000, August 17: Thalassiora spp.:6000, November 22: Akasiwo sanguinea: 640

FIGURE 7: MODIS based red tide index C together with red tide events provided by SPAFPC.

In Figure 7, the MODIS based red tide index, C is quantized with two bits so that the data is represented with white, grey blue and red of pseudo colors. In particular, white pixels are contaminated with clouds. Red color pixels shows red tide suffered areas. In the begging of July, Chattonella Antiqua type of red tide appeared then red tide suffered areas is getting large until August 20. After that, red tide disappeared rapidly. In the late of November, the different type of red tide appeared. The MODIS based red tide index, C shows totally identical to the red tide warning report from SPAFPC.

3.2   Suspended Solid Derived from MODIS
Based on the equation (4), suspended solid is estimated. Through correlation analysis, 667nm of MODIS band shows the highest correlation so that linear regression with MODIS band 13 and insitu data of S measured at the observation tower in the center portion of the Ariake Sea is conducted. Equation (6) shows regressive equation. Table 2 shows the match-up dataset between both.

$$S = \alpha * [Lw(667)]N + \beta \tag{6}$$

Observation Date	412	443	531	667	S
2010/06/02 11:00	0.5549	0.758	1.6932	0.5243	3.2
2010/06/03 12:00	0.697	0.7029	1.5953	0.5707	3
2010/06/09 11:00	0.8175	1.0853	2.0067	0.7259	7.7
2010/07/20 11:00	0.2687	0.3801	1.3053	0.5695	7
2010/07/20 14:00	0.3707	0.3684	0.7593	0.2527	4.1
2010/07/21 13:00	0.4012	0.2148	0.6054	0.1987	4.9
2010/07/22 13:00	0.7987	1.0449	1.984	0.9338	4.5
2010/07/23 13:00	1.0671	1.3122	2.3904	1.4277	10.3
2010/8/6 11:35	0.7874	0.5541	1.2454	0.5381	2.7
2010/8/6 13:10	0.5967	0.5353	1.1487	0.4942	3.1
2010/8/18 13:35	0.5477	0.513	1.0888	0.453	2.5
2010/8/19 11:00	0.6398	0.727	1.7675	0.8588	3.6
2010/8/21 10:50	0.2006	0.2884	0.936	0.2832	2.4
2010/8/21 14:00	0.3947	0.5356	0.9892	0.2442	2.4
2010/8/22 13:10	0.8374	0.8131	1.4261	0.6707	3.6
2010/8/23 13:55	0.5518	0.6825	1.5094	1.0073	11.4
2010/8/25 13:40	0.6758	0.866	1.7356	1.1435	11.9

TABLE 2: The data used for regressive analysis, relation between xxx(nm) channels of MODIS data and insitu data of S (mg m^{-3}) measured at observation tower situated in the center portion of the Ariake Sea

Then the following regressive coefficients and Root Mean Square Error is estimated α = 7.0948, β = 0.6463, RMSE = 2.08758. Using the regressive equation, S is calculated. Some examples of S are shown in Figure 8.

After all, it is possible to remove the same pattern of river water, in particular, from the estimated red tide index, C. Although the estimated red tide index used to show river water pattern, it can be removed using the river water pattern estimated with the regressive equation. Thus an influence due to suspended solid is removed.

(a) July 21   (b) August 18   (c) August 23   (d) November 5
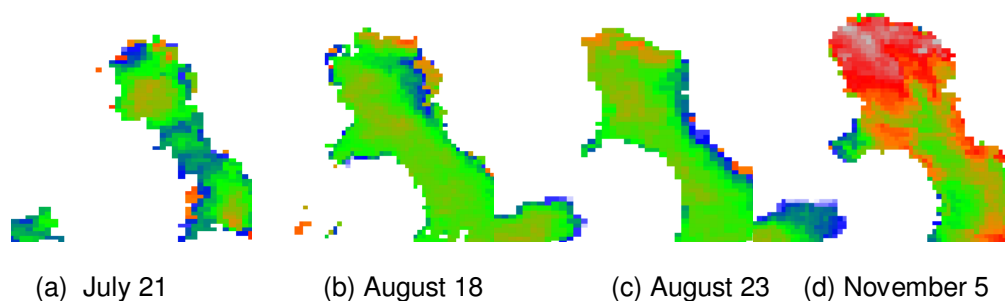
FIGURE 8: Estimated suspended solid pattern derived from the regressive equation

4. CONCLUSIONS

It is confirmed that the proposed method and system for red tide monitoring with camera data with green color filter is effective through laboratory based and at the test site in the field of the Ariake Sea, Kyushu, Japan. Also the proposed method of influence removal due to suspended solid on red tide index measurement with MODIS type of remote sensing imagery data is validated.

5. ACKNOWLEDGEMENT

6. REFERENCES

[1] Dierssen H.M., R.M.Kudela, J.P.Ryan, R.C.Zimmerman, Red and black tides: Quantitative analysis of water-leaving radiance and perceived color for phytoplankton, colored dissolved organic matter, and suspended sediments, Limnol. Oceanogr., 51(6), 2646–2659, E 2006, by the American Society of Limnology and Oceanography, Inc., 2006.

[2] Arnone, R. A., Martinolich, P., Gould, R. W., Jr., Stumpf, R., & Ladner, S., Coastal optical properties using SeaWiFS. Ocean Optics XIV, Kailua Kona, Hawaii, USA, November 10–13, 1998. SPIE Proceedings., 1998.

[3] Stumpf, R. P., Arnone, R. A., Gould Jr., R. W., Martinolich, P. M., & Martinuolich, V., A partially coupled ocean-atmosphere model for retrieval of water-leaving radiance from SeaWiFS in coastal waters. In S. B. Hooker, & E. R. Firestone (Eds.), SeaWiFS Postlaunch Tech. Report Series. NASA Technical Memorandum, 2003-206892, vol. 22 (p. 74), 2003.

[4] Gordon, H. R., & Wang, M., Retrieval of water-leaving radiance and aerosol optical thickness over the oceans with SeaWiFS: A preliminary algorithm. Applied Optics, 33, 443–452, 1994.

[5] O'Reilly, J. E., Maritorena, S., Siegel, D. A., O'Brien, M. C., Toole, D.,Chavez, F. P., et al., Ocean color chlorophyll a algorithms for SeaWiFS, OC2, and OC4: Version 4. In B. Hooker, & R. Firestone (Eds.), SeaWiFS Postlaunch Tech. Report Series. NASA Technical Memorandum 2000-206892, vol. 11 (p. 2000), 2000.

[6] Weijian C., Hall, L.O., Goldgof, D.B., Soto, I.M., Chuanmin H, Automatic red tide detection from MODIS satellite images, Systems, Man and Cybernetics, 2009. SMC 2009. IEEE International Conference on SMC, 2009.

[7] Kohei Arai and Yasunori Terayama, Polarized radiance from red tide, Proceedings of the SPIE Asia Pacific Remote Sensing, AE10-AE101-14, Invited Paper, 2010

[8] Kohei Arai, *Red tides*: combining satellite- and ground-based detection. 29 January 2011, *SPIE Newsroom*. DOI: 10.1117/2.1201012.003267, http://spie.org/x44134.xml?ArticleID=x44134

Kohei Arai & Yasunori Terayama

A Method for Red Tide Detection and Discrimination of Red Tide Type (Spherical and Non-Spherical Shapes of Red Tide) Through Polarization Measurements of Sea Surface

Kohei Arai   *arai@is.saga-u.ac.jp*
Information Science Department
Saga University
Saga City, 840-8502, Japan

Yasunori Terayama   *terra@is.saga-u.ac.jp*
Information Science Department
Saga University
Saga City, 840-8502, Japan

Abstract

A method for red tide detection and for discrimination of red tide type (spherical and non-spherical shapes of red tide type) through polarization measurements of water leaving radiance is proposed. There are a variety of shapes of red tide types, in particular, spherical and non-spherical shapes. Polarization characteristics of spherical and non-spherical shapes of red tide types are different each other resulting in discrimination can be done through polarization measurement. Through laboratory based experiments with Chattonella Antiqua containing water and just water as well as Chattonella Marina and Chattonella Globossa containing water, it is confirmed that the degree of polarization of non-spherical shape of red tide is greater than that of spherical shape of red tide. Also it is confirmed that the polarization measurements is effective for discrimination between spherical and non-spherical shapes of red tide at the coastal areas of the Ariake sea in Kyushu, Japan in comparison to insitu data of red tide with research vessel.

Keywords: Red Tide, Remote Sensing Reflectance, Polarized Radiance, Polarization Camera.

1   INTRODUCTION

Due to red tide contaminations, water color is changed by an algal bloom. In accordance with increasing of phytoplankton concentration, sea surface color changes from blue to green as well as to red or brown depending on the majority of phytoplankton (Dierssen et al, 2006) so that it is capable to detect red tide using this color changes [1].

MODIS ocean color bands data is used for red tide detection. An iterative approach (Arnone et al., 1998 [2]; Stumpf et al., 2003 [3]) for sediment-rich waters, based on the Gordon and Wang (1994) algorithm [4], is used to correct for the atmospheric interference in the six ocean color bands in turbid coastal waters to obtain water leaving radiance, which are then used in the band-ratio algorithm (O'Reilly et al., 2000 [5]) to estimate Chlorophyll in unit of mg m^{-3}. Also suspended solid is estimated with two bands algorithm (visible minus near infrared bands data). The multi-channels of red tide detection algorithms (in the formula of $C=(R_i-R_j)/(R_k-R_l)$ where R_i, R_j, R_k and R_l are the reflectivity derived from bands *i, j, k* and *l*.) are proposed. Also learning approaches based on k-nearest neighbors, random forests and support vector machines have been proposed for red tide detection with Moderate Resolution Imaging Spectroradiometer: MODIS satellite images (Weijian C.,et al.,2009) [6].

Satellite based red tide detection does work under a fine weather condition but not under cloudy and rainy conditions obviously. Furthermore, revisit period of fine resolution of radiometer onboard satellite orbits are longer than typical red tide propagations so that it is not enough

observation frequency if only remote sensing satellite is used for red tide detections. Therefore satellite-and ground-based red tide monitoring system is proposed [7]. In the ground based red tide monitoring system, green colored filtered camera and polarization camera are featured for detection of red tide and discrimination of red tide types [8].

In this paper, a method of which polarization film attached camera images are used for correction of polarization influence on the band-pass filter attached camera images is proposed. Furthermore, an attempt is made for red tide specie discrimination between spherical and non-spherical shapes using ground based polarization camera images.

The second chapter describes the proposed method followed by experiments for validation of the proposed method and system. Then a possibility of red tide detection with polarized radiance measurements is discussed followed by concluding remarks.

2. THE PROPOSED METHOD

2.1 Polarization Measurements for Discrimination of Phytoplankton Types
An attempt is made for red tide specie (phytoplankton type) discrimination between spherical and non-spherical shapes based on polarization measurements. There is a demand of phytoplankton type identification. There are so many types of phytoplankton. Not only pigment, but also shape, size are different each other. Shape of phytoplankton is concerned. For instance, Chattonella Antiqua (ellipsoidal) and Chattonella Globosa (spherical) has the different shape each other as is shown in Figure 1.
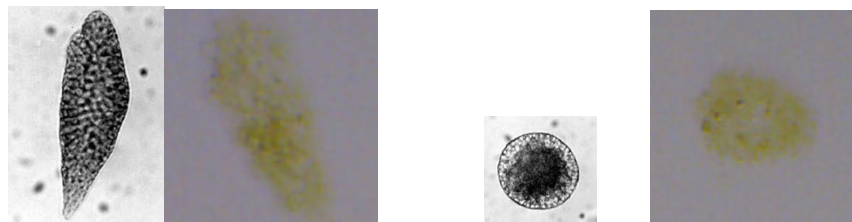
(a) Chattonella Antiqua (b) Chattonella Globosa (c)Chatonella Marina
FIGURE 1: Different type and shape of Chattonella

Size of Chattonella Antiqua is around 50-130 μm x 30-50 μm so that it might show polarization characteristics while Chattonella Globosa does not have any polarization characteristics because it has a spherical shape. Accordingly, polarization radiance reflected from the Chattonella Antiqua is different from that of Chattonella Globosa. In order to confirm this fact, polarization measurement of the sea surface is conducted.

2.2 Experiment in Laboratory
An experiment for discrimination of red tide type between spherical and non-spherical shapes of red tide with polarization measurements is conducted. Outlook of the experiment set-up is shown in Figure.2. Figure 3 shows acquired polarization images for both Chattonella Antiqua contaminated water and just water together with a portion of DP (Degree of Polarization: equation (1)) image and its histogram (ellipsoidal portion of DP image).

$$DP=(Rp-Rs)/(Rp+Rs) \qquad (1)$$

where Rp, Rs denotes radiance of p and s polarization, respectively.

Averaged DP of Chattonella Antiqua contaminated water is 32 while that of just water is 20. As is shown in Figure 1, the shape of Chattonella Antiqua looks like a football and size of Chattonella Antiqua is relatively large so that DP of Chattonella Antiqua contaminated water is greater than that of Chattonella Marina (spherical shape) and Chattonella Globossa (much small spherical

shape) as well as just water. Also DP of Chattonella Marina contained water is measured. The averaged DP is 24 so that it is confirmed that it is possible to discriminate between Chattonella Antique and Marina using polarization measurements.

Through these laboratory based experiments, it is permissive to estimate existence of red tide and also discrimination between non-spherical and spherical shapes of red tide type can be done with polarization measurements of sea surface.
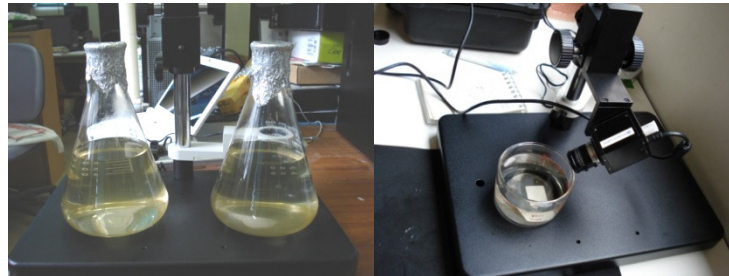
FIGURE 2: Chattonella Antiqua containing water and Chattonella Marina containing water and experimental set-up with polarization camera.

(a) DP of Chattonella Antiqua containing water   (b) DP of just water
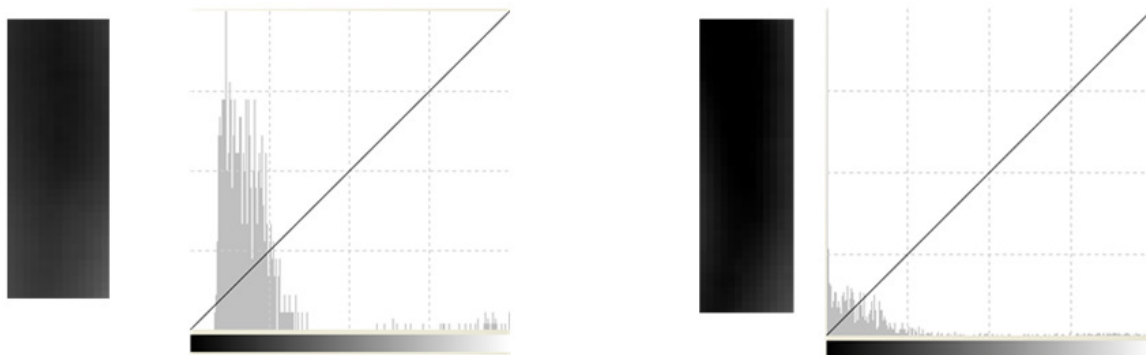
(c) DP image and its histogram of Chattonella Antiqua contaminated water (d) those for water
FIGURE 3: Degree of polarization of Chatonnella Antiqua contaminated water (DP=32) and just water (DP=20)

3. EXPERIMENTS
## 3.1   Intensive Study Area
Figure 4 shows the locations for the ground-based red tide monitoring system stations. Five stations are situated at the seashore of the Ariake Sea in Kyushu Island, Japan where red tide appears almost every year.

Water quality measuring instruments gather the information of chlorophyll-a, suspended solids, water turbidity, hue information of water color, salinity, water temperature, conductivity of the water, etc. On the other hand, weather robot gathers air temperature, relative humidity, atmospheric pressure, wind direction and wind speed, etc.

(a) Locations of red tide monitoring stations   (b) Location of the Ariake Sea
FIGURE 4: Locations of the proposed red tide monitoring system stations (Red circle)
©Google.
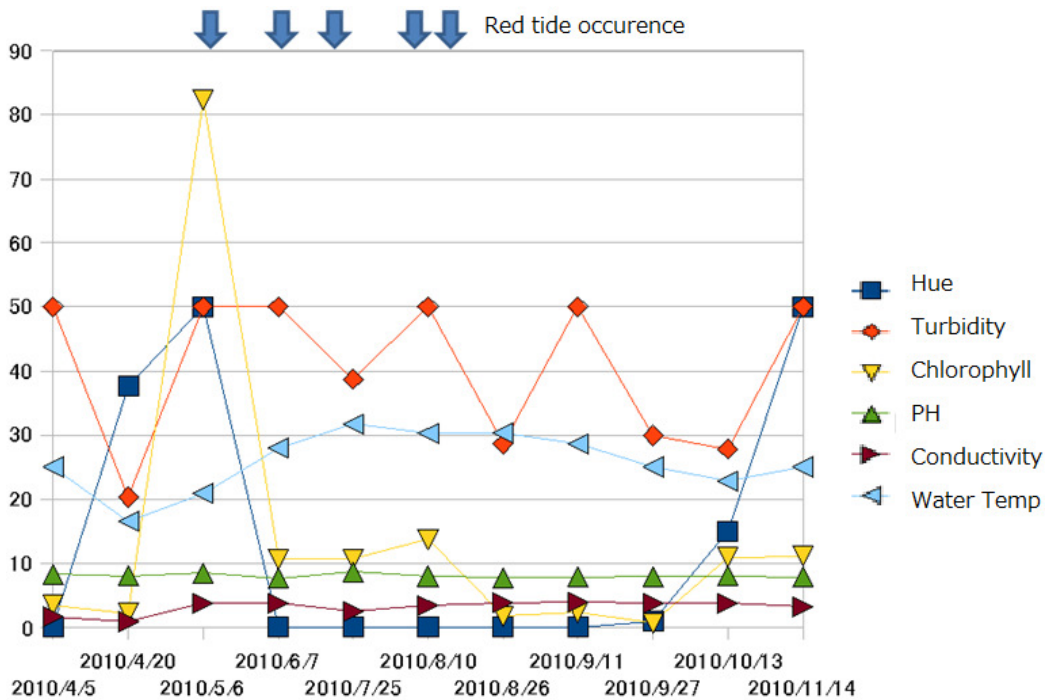
FIGURE 5: Red tide occurrence and measured data for 8 months in 2010.

3.2   Measured data

Figure 5 shows hue, turbidity, chlorophyll, PH, Conductivity, water temperature measured at the Nanaura station for the period from the begging of April 2010 to the middle of November 2010. In

the summer time, sever Chattonella Antique occurred. Other than that, there are so many red tide events in the period as follows,

May 21: Heterosigma:10, Skeletonema spp.:7125
June 25: Heterosigma:100, Skeletonema spp.:6450
July 5: Chattonella Antiqua:480, Chattonella spp.:130
July 20: Skeletonema spp.:88000
August 2: Cript: 18000
August 10: Chattonella Antiqua:1080
August 17: Thalassiora spp.:6000, Skeletonema spp.:7250, Chattonella spp.:1400
November 22: Akasiwo sanguinea: 640
These events are reported by SPAFPC with the date, red tide type and the number of red tide a litter of sea water.

In the same period, polarization camera data are acquired. Figure 6 shows the Histograms of the acquired p and s polarized photos of the sea surface of Nanaura test site of the Ariake sea (From the top, Acquisition date, p or s polarizations, average of the histogram and DP which appear the bottom of the 90 degree of polarization data). Example of the acquired natural color, 0 degree of polarization and 90 degree of polarization of photos are shown in Figure 7. These photos are taken at Nanaura test site on August 10 2010. In particular, the Ariake sea was covered with Chattonella Antiqua of red tide almost entirely.

(a) July 25 and August 10   (b) August 26 and September 11
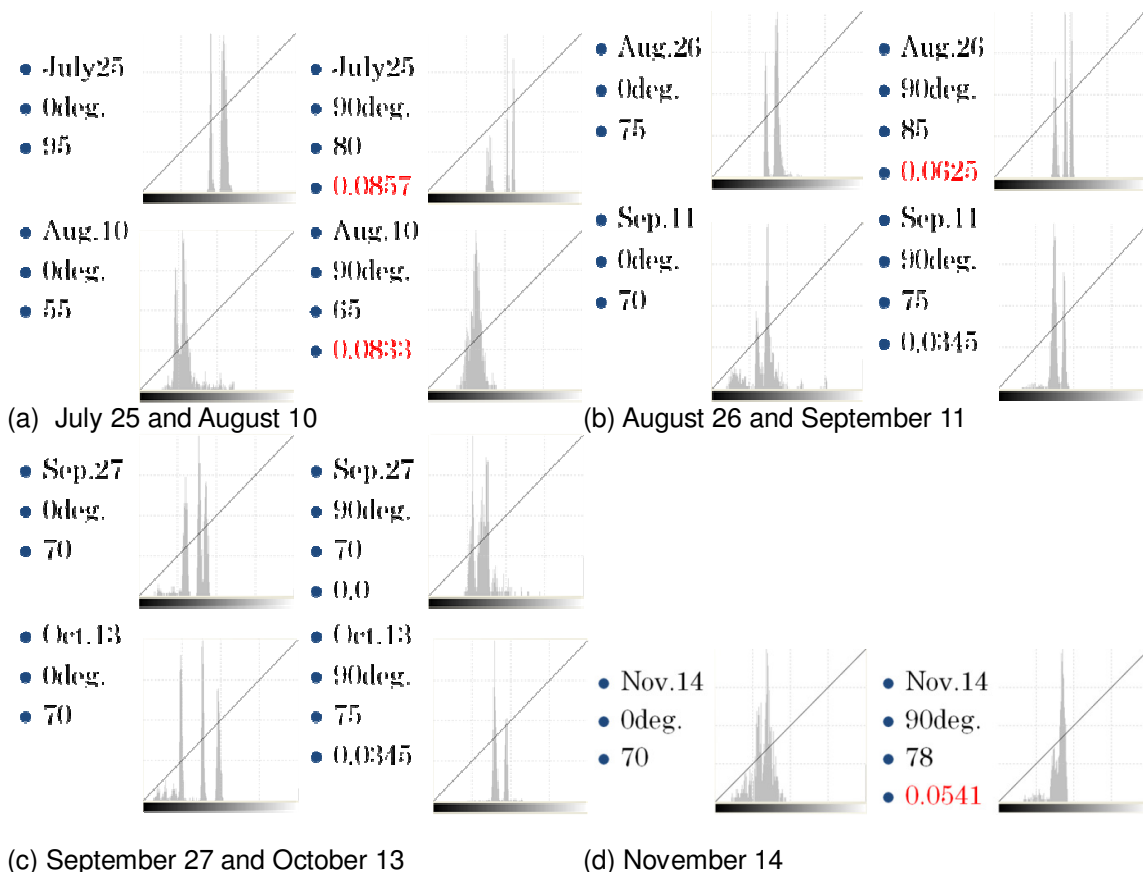
(c) September 27 and October 13   (d) November 14
FIGURE 6: Histograms of the acquired p and s polarized photos of the sea surface of the Nanaura test site of the Ariake sea (From the top, acquisition date, p or s polarizations, average of the histogram and DP which appear the bottom of the 90 degree of polarization data).

(a) Natural photo   **(b) 0 degree of polarization photo**

(c) 90 degree of polarization photo

FIGURE 7: Example of the acquired natural color, 0 degree of polarization and 90 degree of polarization of photos which are taken at the Nanaura test site on August 10 2010.

3.3   Summarized Results

Calculated DP is summarized as follows,

July 25: DP=0.0857, August 10: DP=0.0833, August 25: 0.0625, September 11: 0.0345, September 27: 0.0, October 13: 0.0345, November 14:0.0541

Relation between red tide measured by Saga Prefectural Ariake Fisheries Promotion Center: SPAFPC and the calculated DP is as follows,

May 21: Heterosigma:10, Skeletonema spp.:7125
June 25: Heterosigma:100, Skeletonema spp.:6450
July 5: Chattonella Antiqua:480, Chattonella spp.:130
July 20: Skeletonema spp.:88000→DP=0.0857
August 2: Cript: 18000
August 10: Chattonella Antiqua:1080→DP=0.0833
August 17: Thalassiora spp.:6000, Skeletonema spp.:7250, Chattonella spp.:1400→DP=0.0625
September 11, September 27, October 13→DP=0.0345, 0.0, 0.0345
November 22: Akasiwo sanguinea: 640→DP=0.0541

SPAFPC picked sea water up from their research vessel and then red tide type is identified and the number of red tide is counted by using microscopic instrument. They used to provide caution

of red tide to fisherman together with suffered area map including red tide type and the number of red tide. Figure 8 shows an example of the caution provided on July 5 and August 10 2010.
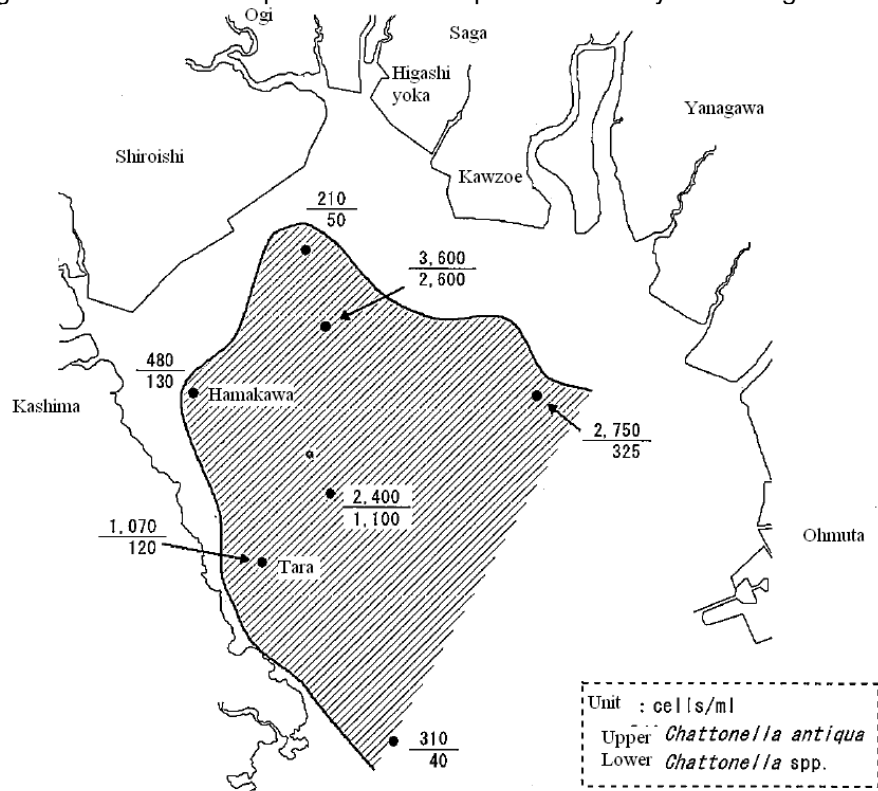
(a) Measured at 8:15-9:45 on August 10 2010
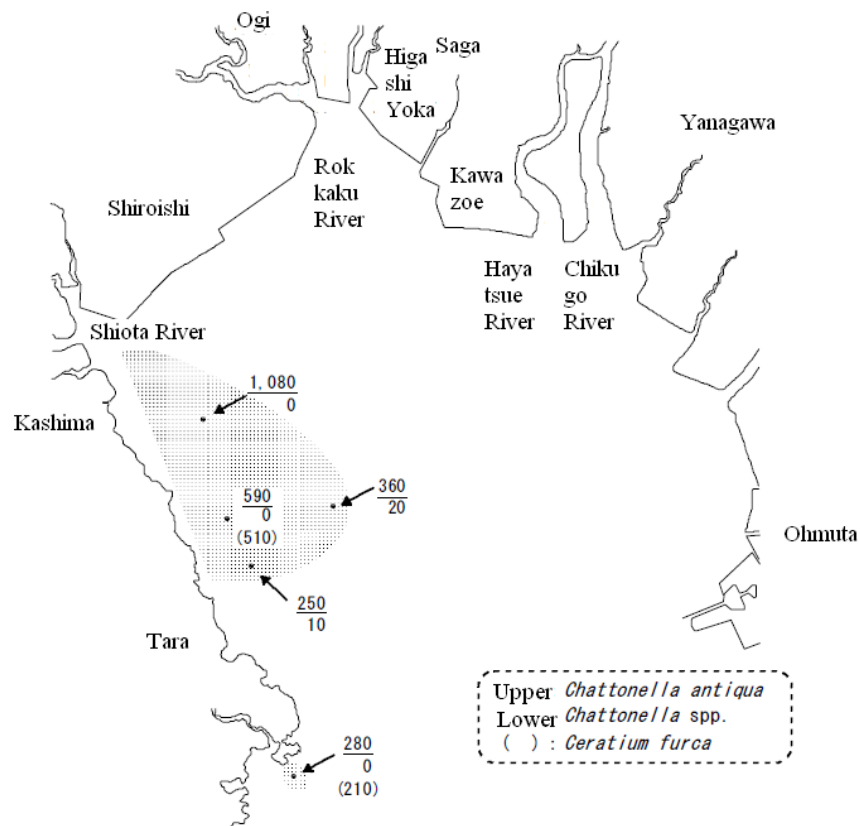
(b) Measured at 13:30-15:30 on July 5 2010
FIGURE 8: SPAFPC provided red tide caution with red type and the number of red tide

SPAFPC uses their research vessel so that they cannot measure red type and the number of red tide near to coastal areas while the proposed red tide monitoring system allows measurements in particular in coastal area so that these can be used complementally.

4. CONCLUSIONS

The proposed polarization characteristics based method for red tide detection is validated in both of laboratory basis as well as field experiment basis. It is confirmed that Degree of Polarization: DP of red tide contained water is greater than that of just water in laboratory basis. Meanwhile a strong relation between insitu measurement data provided by Saga Prefectural Ariake Fisheries Promotion Center and the measured DP proposed in this paper is also confirmed with field experimental data which are acquired at the Ariake Sea in Kyushu, Japan where red tide occurs almost every year. The proposed method requires polarization film attached camera so that it is quit cheap and easy to equip. Furthermore, red tide type discrimination with polarized radiance measurements is attempted. Through a comparison of DP between Chattonella Antiqua containing water and water from water supply, it is confirmed that the former is greater than the later. Non-spherical shape of red tide can be discriminated with the other types of red tide (Spherical shape).

5. ACKNOWLEDGEMENT

Science, Saga University for his nice discussions and providing the Chattonella Antique and marina containing water.

6. REFERENCES

[1]   Dierssen H.M., R.M.Kudela, J.P.Ryan, R.C.Zimmerman, Red and black tides: Quantitative analysis of water-leaving radiance and perceived color for phytoplankton, colored dissolved organic matter, and suspended sediments, Limnol. Oceanogr., 51(6), 2646–2659, E 2006, by the American Society of Limnology and Oceanography, Inc., 2006.

[2]   Arnone, R. A., Martinolich, P., Gould, R. W., Jr., Stumpf, R., & Ladner, S., Coastal optical properties using SeaWiFS. Ocean Optics XIV, Kailua Kona, Hawaii, USA, November 10–13, 1998. SPIE Proceedings., 1998.

[3]   Stumpf, R. P., Arnone, R. A., Gould Jr., R. W., Martinolich, P. M., & Martinuolich, V., A partially coupled ocean-atmosphere model for retrieval of water-leaving radiance from SeaWiFS in coastal waters. In S. B. Hooker, & E. R. Firestone (Eds.), SeaWiFS Postlaunch Tech. Report Series. NASA Technical Memorandum, 2003-206892, vol. 22 (p. 74), 2003.

[4]   Gordon, H. R., & Wang, M., Retrieval of water-leaving radiance and aerosol optical thickness over the oceans with SeaWiFS: A preliminary algorithm. Applied Optics, 33, 443–452, 1994.

[5]   O'Reilly, J. E., Maritorena, S., Siegel, D. A., O'Brien, M. C., Toole, D.,Chavez, F. P., et al., Ocean color chlorophyll a algorithms for SeaWiFS, OC2, and OC4: Version 4. In B. Hooker, & R. Firestone (Eds.), SeaWiFS Postlaunch Tech. Report Series. NASA Technical Memorandum 2000-206892, vol. 11 (p. 2000), 2000.

[6]   Weijian C., Hall, L.O., Goldgof, D.B., Soto, I.M., Chuanmin H, Automatic red tide detection from MODIS satellite images, Systems, Man and Cybernetics, 2009. SMC 2009. IEEE International Conference on SMC, 2009.

[7]   Kohei Arai and Yasunori Terayama, Polarized radiance from red tide, Proceedings of the SPIE Asia Pacific Remote Sensing, AE10-AE101-14, Invited Paper, 2010

[8]   Kohei Arai, *Red tides*: combining satellite- and ground-based detection. 29 January 2011, *SPIE   Newsroom*.   DOI: 10.1117/2.1201012.003267, http://spie.org/x44134.xml?ArticleID=x44134

Kohei Arai, Nagamitsu Ohgi, Fumihiro Sakuma, Masakuni Kikuchi, Satoshi Tsuchida & Hitomi Inada

Trend Analysis of Onboard Calibration Data of Terra/ASTER/VNIR and One of the Suspected Causes of Sensitivity Degradation

Kohei Arai   *arai@is.saga-u.ac.jp*
Information Science Department
Saga University
Saga City, 840-8502, Japan

Nagamitsu Ohgi   *nohgi@jaros.or.jp*
Japan Resources Observation System and Space Utilization Organization,
2-24-2 Nichibei Bldg, Hacchobori, Chuo, Tokyo, 104-0032 Japan

Fumihiro Sakuma   *sakuma@jaros.or.jp*
Japan Resources Observation System and Space Utilization Organization,
2-24-2 Nichibei Bldg, Hacchobori, Chuo, Tokyo, 104-0032 Japan

Masakuni Kikuchi   *kikuchi@jaros.or.jp*
Japan Resources Observation System and Space Utilization Organization,
2-24-2 Nichibei Bldg, Hacchobori, Chuo, Tokyo, 104-0032 Japan

Satoshi Tsuchida   *s.tsuchida@aist.go.jp*
Advanced Industrial Science and Engineering,
1-1-1 Umezono, Tsukuba, Ibaraki 305-8568 Japan

Hitomi Inada   *hinada@bx.jp.nec.com*
NEC Corporation,
1-10 Nisshin, Fuchu, Tokyo 183-8501 Japan

Abstract

Sensitivity degradation trend is analyzed for ASTER: Advanced Spaceborne Thermal Emission and Reflection radiometer/Visible and Near-Infrared Radiometer: VNIR onboard Terra satellite. Fault Tree Analysis is made for sensitivity degradation. Firstly, it is confirmed that the VNIR detectors are stable enough through dark current and shot noise behavior analysis. Then it is also confirmed that radiance of calibration lamp equipped VNIR is stable enough through lamp monitor of photodiode output data analysis. It is confirmed that radiance at the front of VNIR optics is, on the other hand, degraded in conjunction with sensitivity degradation of VNIR through an analysis of another photodiode output data which is equipped at the front of VNIR optics, photodiode output is scale-off at around one year after the launch though. VNIR optics transparency might not be so degraded due to the fact that VNIR output and the later photodiode output show almost same degradations. Consequently, it may say that one of possible causes of VNIR sensitivity degradation is thruster plume.

Keywords: ASTER, Onboard Calibration, Vicarious Calibration, Plume Impingement.

1. INTRODUCTION

Almost all the solar reflection channels of mission instruments onboard Earth observation satellite carry their own calibration system to maintain consistency of the radiometric fidelity of the instrument. Thus users may convert from the Digital Number, DN to radiance taking the onboard calibration system derived calibration coefficient into account. There are some reports on the calibration issues which include the MOS-1: Marine Observation Satellite-1[1], Landsat-7 ETM+: Enhanced Thematic Mapper Plus[2], SeaWiFS: Sea-viewing Wide Field-of-view Sensor[3],

Kohei Arai, Nagamitsu Ohgi, Fumihiro Sakuma, Masakuni Kikuchi, Satoshi Tsuchida & Hitomi Inada

SPOT-1 and 2: Satellite Pour l'Observation de la Terre[4], Hyperion[5], and POLDER: POLarization and Directionality of the Earth's Reflectance[6]. Onboard calibrators cannot provide results of a higher accuracy than the preflight laboratory calibration. This means that the accuracy of the in-flight (absolute) calibration is inferior to the preflight results. This is because the preflight calibration source is used to calibrate the onboard calibrators. In addition, the uncertainty of the onboard calibrator typically increases with time. Hence, it makes good sense to include additional calibration approaches that are independent of the preflight calibration. Besides the normal and expected degradation of the onboard calibrators, they also run the risk of failing or operating improperly. Therefore, vicarious approaches are employed to provide further checks on the sensor's radiometric behavior. Any electro-optical sensor is expected to degrade once in orbit, and therefore requires a mechanism to monitor the data's radiometric quality over time. Many sensors, including ASTER: Advanced Spaceborne Thermal Emission and Reflection radiometer, employ onboard calibration devices to evaluate temporal changes in the sensor responses. Onboard calibrators, in general, provide excellent temporal sampling of the sensor's radiometric behavior over time. In addition, the repeatability and precision of the onboard systems allow use of these data in characterizing the sensor's response trends. Typical approaches for onboard calibration include lamp-based, diffuser-based, and detector-based methods. ASTER VNIR: Visible and Near-Infrared Radiometer and SWIR: Short Wave Infrared Radiometer use lamp based onboard calibrators. The specific design of the ASTER OBC: Onboard Calibrator is described in the following section. Then the sensor's response trends and suspected influence due to plume impingement of contamination of optics entrance of ASTER instrument is followed by with some evidences. Finally, discussions and concluding remarks are described.

2. ONBOARD CALIBRATION SYSTEM OF TERRA/ASTER/VNIR
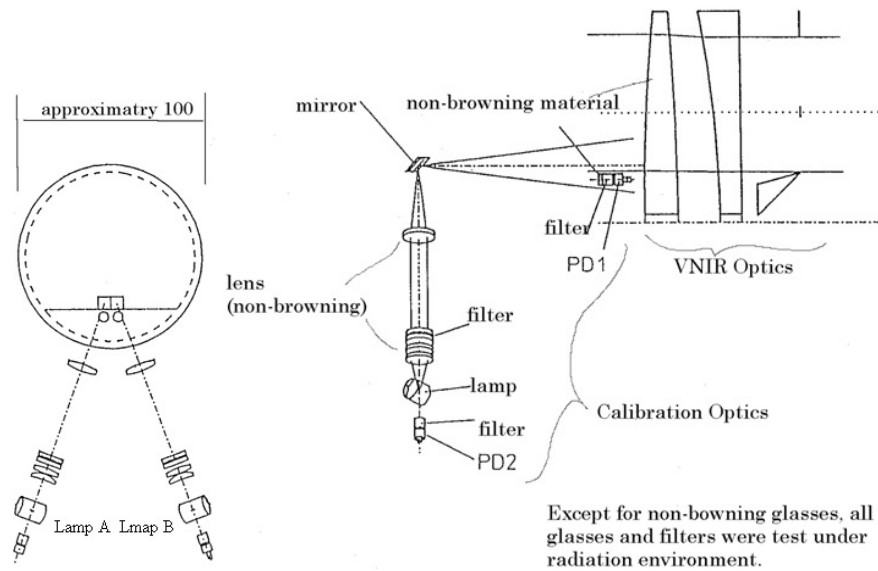
2.1 Onboard Calibration System

ASTER VNIR and SWIR channels use lamp-based onboard calibrators for monitoring temporal changes in the sensor responses. Space restrictions aboard the Terra platform disallow a solarbased calibration, and therefore, onboard calibration is lamp-based. The VNIR and SWIR have two onboard calibration lamps, lamp-A and lamp-B. Both are used periodically, and as a backup system. The VNIR calibration lamp output is monitored by a silicon photo monitor, and is guided to the calibration optics. The calibration optics output illuminates a portion of the VNIR aperture's observation optics and is monitored by a similar photo monitor. Meanwhile, the SWIR calibration assembly does not have a second silicon photo monitor. In the pre-flight phase, the onboard calibrators were well characterized with integration spheres calibrated with fixed freezing point blackbodies of Zn (419.5K). This was accomplished by comparing the VNIR and SWIR output derived from the integration sphere's illumination of the two sensors. The same comparison was made by the calibration lamp's (A and B) illumination of the two sensors. Next, the pre-flight gain and offset data (no illumination) were determined. In addition, MTF: Modulation Transfer Function was measured with slit light from a collimator while stray light effect was measured with the integration sphere illumination, which is blocked at the full aperture of the VNIR and SWIR observation optics entrance. The pre-flight calibration data also includes

(1) spectral response,
(2) out-of-band response.

The VNIR has two onboard calibration halogen lamps (A and B) as is shown in Figure1. The light from these lamps is led to the VNIR optics via a set of calibration optics. Filters and photomonitors are located fore and aft of the calibration optics to monitor the output of the lamps as well as any possible degradation in the calibration optics. Lamp output and photo monitor data are collected every 33 days (primarily it was 16 days of the Terra orbital revisit cycle plus one day = 17 days and is 49 days now a day), and RCC: Radiometric Calibration Coefficients are calculated from the VNIR output taking into account the photo-monitor output. The RCC values are normalized by the pre-flight data to determine their final estimate. This procedure is the same for the SWIR RCC calculation except that the SWIR OBC does include a photo monitor system at the lamp but does not include a photo monitor system for entrance of the optics. Thus, only data

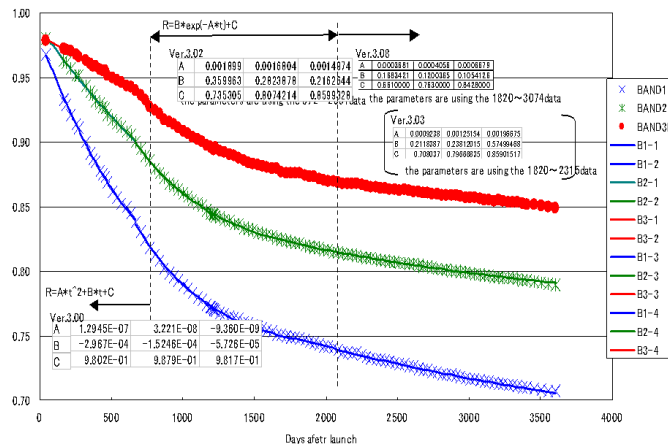from a photo monitor that is aft of the calibration lamp is taken into account.

FIGURE 1: Onboard calibration system of the ASTER/VNIR

2.2 Onboard Calibration Trend
Figure2 shows the RCC trends for VNIR.

OBC RCC

FIGURE 2: OBC RCC trends for Band 1(Blue), Band 2(Green) and Band 3(Red)

The RCC were changed relatively rapidly in the early stage of the launch, and is changed gradually for the time being. These are approximated with an exponential function with a bias and a negative coefficient. If the trend is approximated with the function of RCC = B exp (-At) + C, then A, B, and C equal the following values: Band1 (560nm): A = 0.00190, B = 0.360, C = 0.735 Band2 (660nm): A = 0.00168, B = 0.282, C = 0.807Band3 (810nm): A = 0.00150, B = 0.216, C = 0.860 During 2500 days after the launch, VNIR OBC RCC were degraded about 10% for Band3, 16% for Band2 and 23 % for Band1, respectively while SWIR OBC RCC were degraded approximately 2.0 to 3.5% depending on bands[7]. These trends are very similar to the vicarious calibration derived RCC, and also look similar to the OBC RCC trend of the OPS: Optical Sensor onboard the JERS-1: Japanese Earth Resources Satellite, a legacy precursor to the ASTER instrument. There are two major trends in OBC RCC trends, at the first 800 days and at the 2100

Kohei Arai, Nagamitsu Ohgi, Fumihiro Sakuma, Masakuni Kikuchi, Satoshi Tsuchida & Hitomi Inada

days after the launch as is shown in Figure2. It is suspected that out-gas from the materials of VNIR instrument and thruster plume in the initial phase. Each of the VNIR bands is shown, as are the onboard calibrator results for these bands in a fashion similar to that shown in Figure 2. On the other hand, Figure 3 shows vicarious calibration trend [8]. Although both onboard and vicarious calibration trends are similar, there are small biases, a few percents for Band 1 to 3N as is indicated in Figure 3. Therefore, VNIR sensitivity degradation is confirmed with the different two sources. VNIR sensitivity degradation can be expressed with exponential function so that one of the possible causes of the degradation is contamination. The other causes are degradation of optical transparency of the calibration optics, sensitivity degradation of photo-monitor, degradation of photmonitor filter, etc.
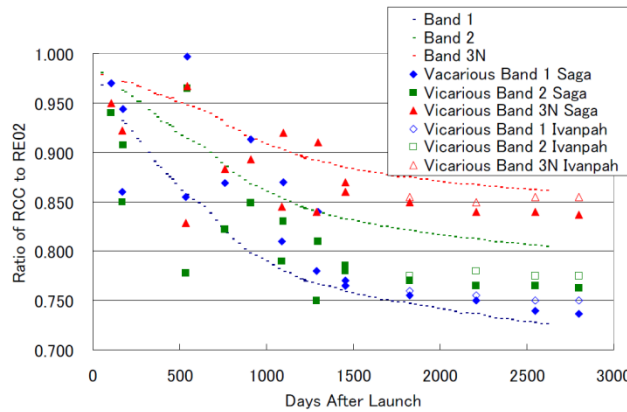
FIGURE 3: OBC and Vicarious RCC Trends

2.3 Photo-Monitor Output Trend
As is shown in Figure 1, VNIR has two photo-monitors, one (PD2) is set at lamp output and the other one (PD1) is set at the optics entrance, just in front of the collecting mirror.

Although PD1 output shows scale-off at around 370 days after launch as is shown in Figure 4, the degradation of the degradation ratio shows almost same trend as OBC and vicarious RCC trends. Also PD2 output shows stable lamp illumination so that one of possible causes for the sensitivity degradation is contamination at the optics entrance because the calibration optics is composed with browning lenses (less degradation of transparency due to radiation from solar flare). From the PD1 output data, approximated exponential function is estimated with least square method. The degradation rate is confirmed to be almost same as OBC and vicarious RCC trends as is shown in Figure 5.
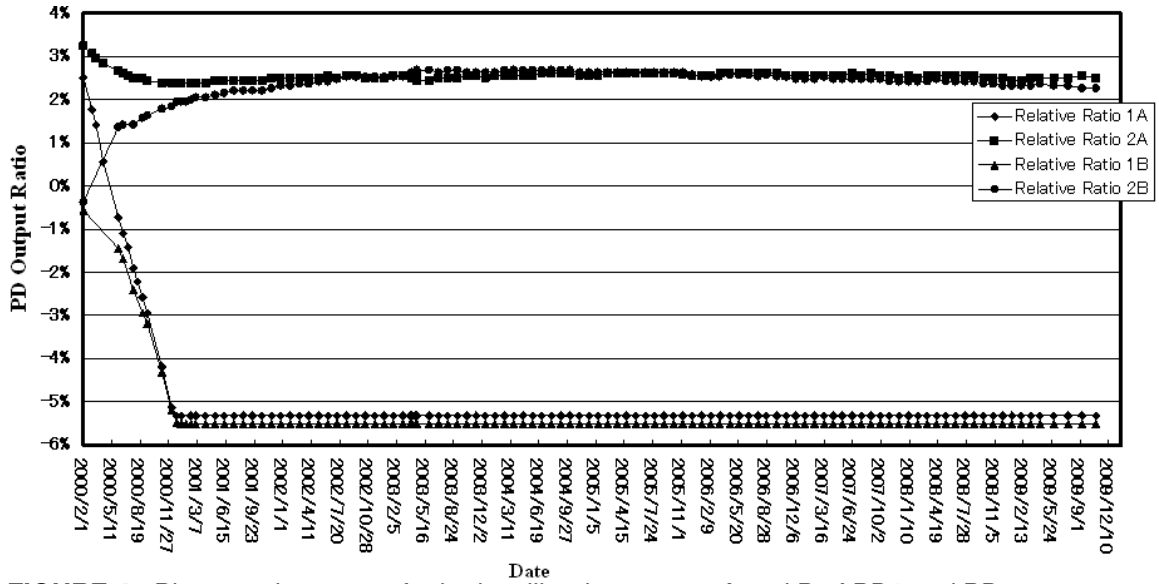
Kohei Arai, Nagamitsu Ohgi, Fumihiro Sakuma, Masakuni Kikuchi, Satoshi Tsuchida & Hitomi Inada

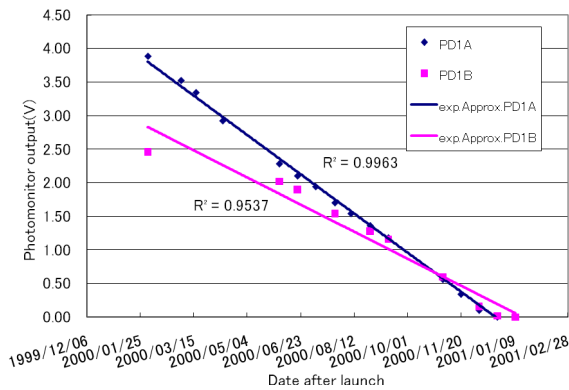**FIGURE 4 :** Photomonitor output for both calibration system A and B of PD1 and PD2.

FIGURE 5 : Approximated exponential function of PD1 output using PD1 data taken in 370 days after launch together with the other photomonitor output trends.

R square for this exponential approximation for PD1A is 0.9963 so that exterpolation might be possible accurately. OBC RCC trends with reference to the calibration systems (Lamp A and B as well as photo-monitor PD1 and 2) are shown in Figure 6. In the figure, exterpolation curve is shown as "pd1a(Exterpolation)", photomonitor output voltage shows negative for the period 370 days after launch though.

Kohei Arai, Nagamitsu Ohgi, Fumihiro Sakuma, Masakuni Kikuchi, Satoshi Tsuchida & Hitomi Inada
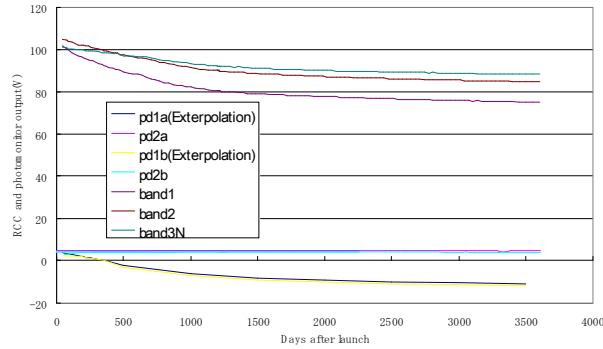

**FIGURE 6 :** OBC RCC trend together with photo-monitor output trend.

The first three lines are for Band 3, 2 and 1, respectively, of RCC ranges from 105 (just after the launch) to 76 at around 3600 days after launch while the last four lines are for photo-monitor output. As is mentioned before, photo-monitor PD1 for both lamp A and B were in scale off at 370 days after launch so that PD1 (lamp A and B) trend were extrapolated by the exponential function with coefficients determined from the PD1 output data of the first 370 days. As is shown in Figure 6, the coefficients of exponential function of RCC trend is almost same as that of exterpolation function of PD1. Thus it might be concluded that one of the possible causes of the RCC degradation would be contamination at the optics entrance of VNIR due to plume impingement. Thruster plume of hydrazine hydrate has not only absorption band at around 12mm but also continuous absorption in the visible region (absorption coefficient is not large though)[1]. Also hydrazine absorption in visible wavelength region is reported [9]. They measured spectral absorption of liquid as a product of hydrazine [10] with several chemicals. Consequently, they found the very calm peak absorption at around 460-480nm. For these reasons, there is a little absorption in visible wavelength region due to hydrazine hydrate of thruster plume which may affect to degradation of optics transparency of mission instruments onboard satellites.

2.4 Possible Causes of Sensitivity Degradation and Fault Tree Analysis
Firstly, it is shown that VNIR detector sensitivity is stable. As is shown in Figure 7 and 8, dark signal (Output signal when no input from the VNIR optics entrance (Night time observation)) and detector temperature is very stable so that it may say that detector sensitivity is stable enough.

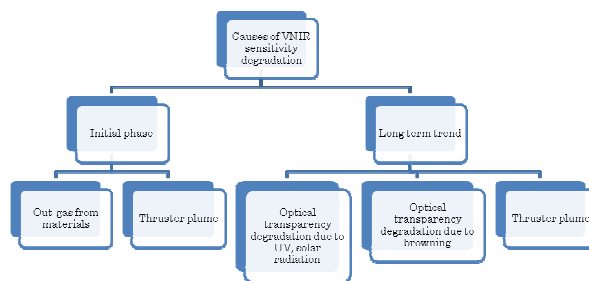[1] http://www.coe.ou.edu/sserg/web/Results/EPA%20Spectra/N2H4%20etc.pdf
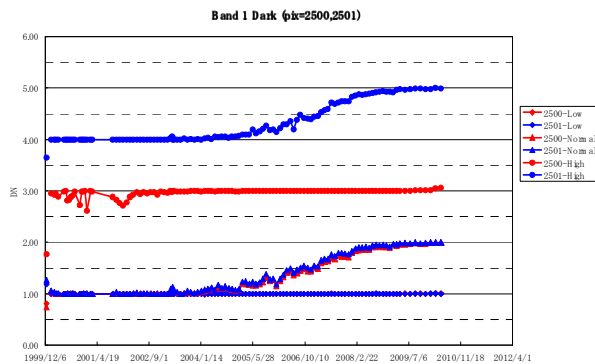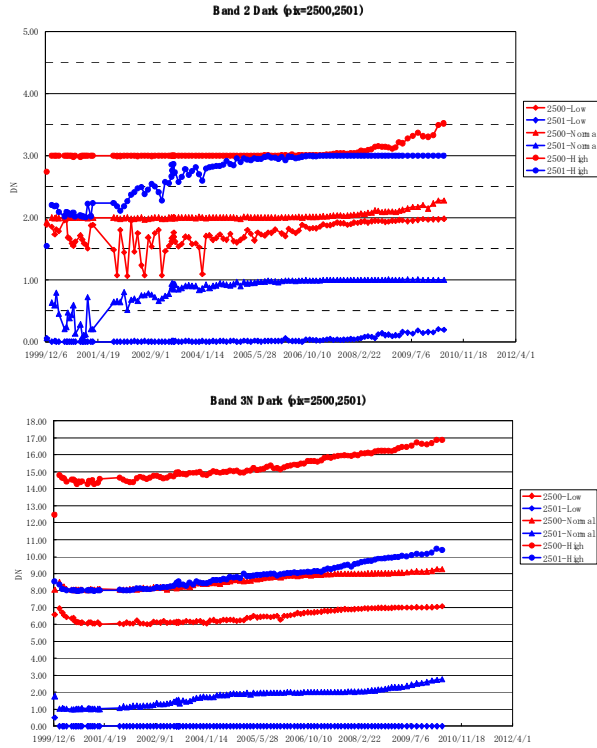
FIGURE 7: Dark signals for Bands 1(Top), 2(Middle), 3(Bottom)
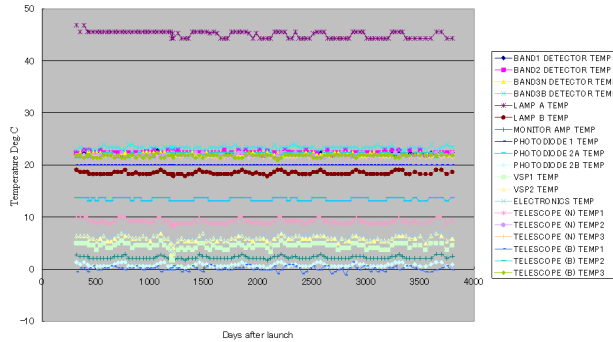
FIGURE 8: Detector temperature for Bands 1,2,3.

As is shown in Figure 4, radiance from the calibration lamp is also stable so that optical transparency of VNIR optics might be degraded. There are some possible causes of the VNIR optical transparency degradation those are (1) Initial phase and (2) Long term sensitivity degradations. In the initial phase, out-gas from materials of VNIR is one of them followed by thruster plume contamination. For the long term degradation, optical transparency degradation due to ultra-violet and solar radiation as well as thruster plume is major causes. Optical transparency degradation due to ultra-violet light polymerization of optics is one of those followed by browning of optics. Fault Tree is shown in Figure 9.

Kohei Arai, Nagamitsu Ohgi, Fumihiro Sakuma, Masakuni Kikuchi, Satoshi Tsuchida & Hitomi Inada

FIGURE 9: Fault Tree for VNIR sensitivity degradation

VNIR optics employs non-browning materials so that it may not occur browning in the optics. Ultra-violet light polymerization of optics might be occurred. It used to be occurred due to organic gas contamination on optics surface, in particular, coating material of the sensor optics onboard satellite[11].

Although VNIR does not employ such coating material at all, it is difficult to say it is not a cause. Thus thruster plume is one of possible causes.
During hydrazine is burning from thruster, plume includes not only hydrazine, N_2H_4, but also NH_3, H_2O, N_2, H_2. Mass fraction of N_2 is dominant followed by NH_3. Terra satellite carries two types of monopropellant of thruster, 5lbf and 1lbf. Plume impingement rate at aperture of NH_3 is dominant followed by H_2O and N_2H_4. Re-emission rate for these molecules are greater than impingement rate so that the surface of the VNIR optics is not accumulate anything. Hydrazine hydrate stick[2] on the surface of optics would occur so that it is suspected that some mixture of hydrazine such as $H_4N_2 \cdot H_2O$ is remained on the surface of VNIR optics (sticking fraction of N_2H_4 is 0.1% in accordance with the site of footnote below 2).

Although hydrazine hydrate has no absorption in visible and near infrared wavelength region, transparency in that region is not 100%. Transparency of $H_4N_2 \cdot H_2O$ is 96% at around VNIR Band 1, 97% at around Band 2 and 98% at around Band 3, respectively. This situation is much severe for short wave infrared region, SWIR. Sensitivity degradation of SWIR is not so significant and is much less than VNIR. One of the reasons for this is that thruster plume is situated in front of optics as a particle, it is not realistic though. Thus sticking hydrazine hydrate on the optics might not be a suspect so that ultra-violet light polymerization of optics might be a suspect. Further investigation is needed.

2.5 Size Distribution of Thruster Plume
From the wavelength dependency of OBC RCC trend, it is possible to estimate size distribution if it is assumed that plume impingement is one of possible causes of the RCC degradation [12],[13]. Figure 10 shows wavelength dependency of the RCC degradations. From this spectral dependency, size distribution is estimated with the assumption that the size distribution is followed by the power law as well as the accumulated number of particles is normalized by one. Figure 11 shows the estimated size distribution. The size distribution estimation has not been validated yet.

---

2 http://www.gps.caltech.edu/genesis/Thrusters.html
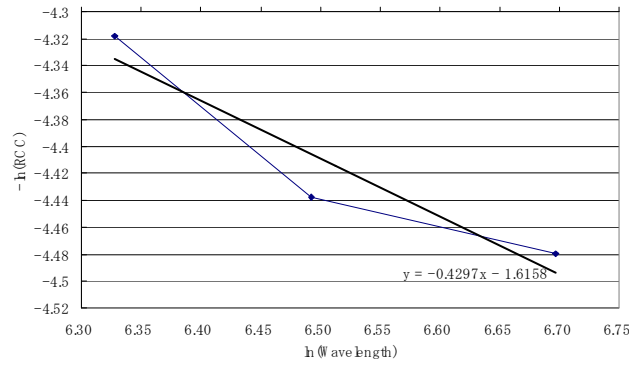
FIGURE10: Spectral characteristics of RCC and its linearly approximated function.
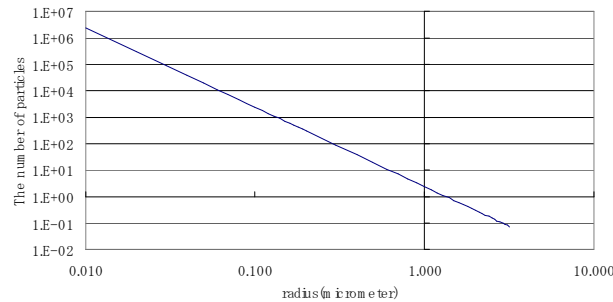
FIGURE11: Estimated size distribution of plume impingement that is one of causes of the RCC degradation

### 2.6 Size Distribution and SWIR Sensitivity Degradation
From Figure 11, it can be assumed that hydrazine hydrate is distributed at the optics surface sparsely because most of hydrazine hydrate particle size is smaller than 1 micrometer and the number of the particles with 0.1 micrometer of radius is around 2000 while the number of particle with 0.01 micrometer of radius is 2 million. On the other hand, SWIR sensitivity degradation for each band is around 1.2%, 2.7%, 2.7%, 2.5%, 2.4%, and 2.7% for Band 4-9 within the first 7 and half years after the launch. Meanwhile, the center wavelength of SWIR of each band is 1.65, 2.165, 2.205, 2.26, 2.33 and 2.395 micrometer for Band 4-9 so that hydrazine hydrate particles are small enough for influencing to optics transparency through scattering. It is said that hydrazine hydrate particles do not affect to the sensitivity degradation for SWIR wavelength regions.

2.7 Fuel Consumption and RCC Trend
Another evidence of the causes of RCC degradation is the relation between fuel consumption and RCC degradation. Figure 12 shows the fuel consumption of Terra satellite which carries ASTER/VNIR. Figure 12 also shows approximated function of the fuel consumption together with approximated function of RCC degradation. As is well known that the fuel consumption in just after launch is relatively large, there is bias between the two approximated functions of fuel consumption and RCC degradation. Both functions, however, show almost same trend.

Figure 13 also shows the OBC RCC trends, with the reference to the two calibration systems, Lamp A and B as well as PD2, for Band 1, 2 and 3. Figure13 also shows the fuel consumption and its approximated function with exponential function. It may say that theses show almost same trend.
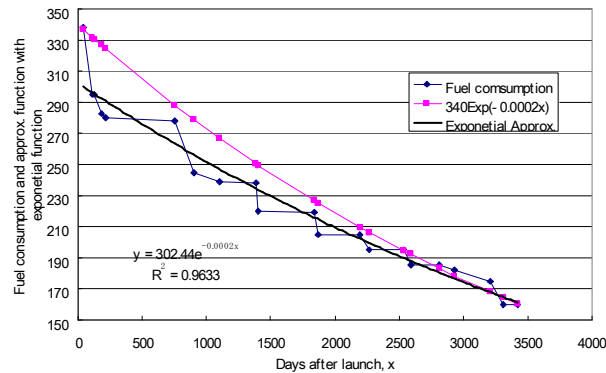
FIGURE 12: The relation between fuel consumption and RCC degradation.
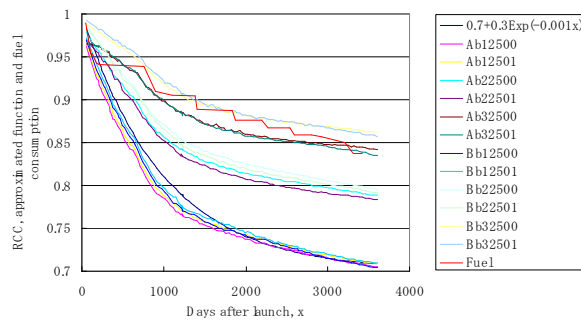
FIGURE 13: Relations between OBC RCC trend and fuel consumption as well as the approximated function of fuel consumption.

2.8 Comparison between Terra/MODIS and VNIR Sensitivity Degradations

Also sensitivity degradation of VNIR is compared to that of Terra/MODIS: Moderate Resolution Imaging Spectroradiometer because ASTER/VNIR and MODIS is onboard and their optics is equipped at Earth pointed plane on the same satellite, Terra so that almost same thruster plume influence may occur for both optics.

Sensitivity degradation of MODIS is well reported[13] so that it is compared to that of VNIR. There are three obvious epochs on around 520, 900 days and 1400 days after launch in terms of coincidence between fuel consumption and sensitivity degradation. These are common to both mission instruments, VNIR and MODIS.

Also these sensitivity degradations for both show coincident to the fuel consumption. Also according to X. Xiong et.al (2006), sensitivity degradation ratio between MODIS bands 8(412nm) and 4(554nm) as well as bands 4 and 17(905nm) are approximately 5.5 and 6.0, respectively. Meanwhile, sensitivity degradation ratio between VNIR and 1(560nm) and 3(810nm) is around 2.2. On the other hand, sensitivity degradation of MODIS band 4 is around 6% at 1500 days after launch while that of VNIR band 1 is 24%. Sensitivity degradation of VNIR is much significant than MODIS.

2.9 RCC Comparison between VNIR Band 3N and 3B

VNIR has two telescopes, band 1, 2 and 3N (Nadir looking) and band 3B (Backward looking) as is illustrated in Figure 14. Both telescope are equipped at the different location with the different angle (3N is pointing to the nadir while 3B is pointing to off-nadir with 27.6 degree). Contamination situations for both telescopes, therefore, are different. For this reason, sensitivity degradations for these two may be different. Figure 15 shows the difference between vicarious calibration data derived RCC for both. Because Band 3B does not have any onboard calibration system so that only vicarious calibration data derived RCC is discussed. If the thruster plume comes from the front of optics uniformly, then contamination of backward optics is 11.38%

(cos(27.6 degree)) less than nadir optics. Both degradations show 8.54% difference between Band 3N and Band 3B so that it is close to 11.38% of less contamination of backward telescope of Band 3B due to thruster plume.
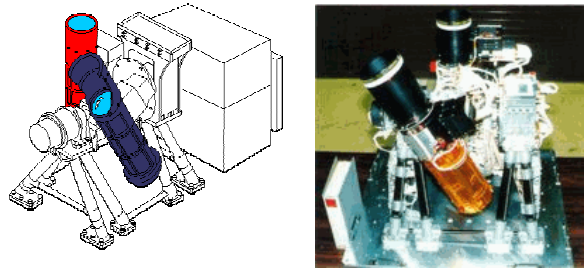
FIGURE 14: Illustrative view of VNIR instrument.
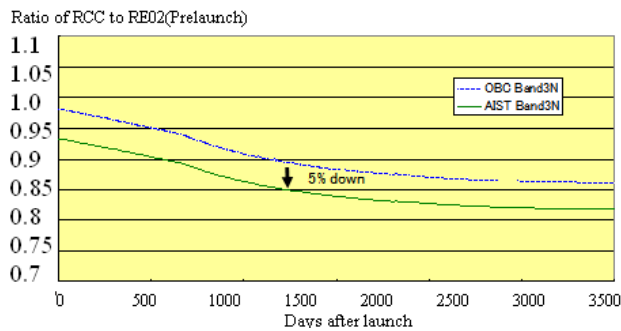
(a) OBC and vicarious RCC trends for Band 3N

(b) Vicarious RCC trend for Band 3B

FIGURE 15: Difference of OBC RCC and vicarious calibration data derived RCC for both Band 3N and Band 3B.

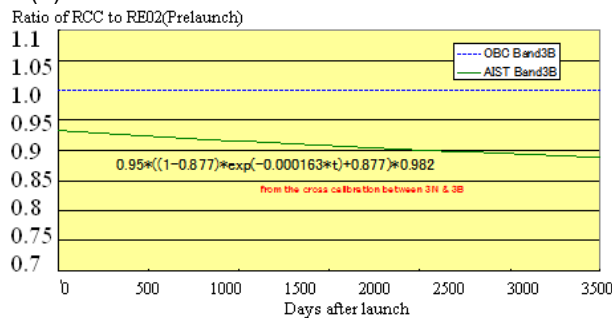Consequently, optics transparency seems to be most suspected cause of the RCC (sensitivity) degradation due to plume impingement by hydrazine hydrate from the thrusters.

2.10 Another Evidence of Contamination of ASTER/TIR Optics With Thruster Plume
ASTER composed with three mission instruments, VNIR, SWIR and Thermal Infrared Radiometer (TIR) which has five spectral channels in the atmospheric window. Sensitivity degradation of TIR Band 12 (9.1 micrometer of spectral channel) is significant followed by the Band 10, 11 as well as Band 13 and 14 as is shown in Table 1. Table 1 shows wavelength coverage and annual degradation of sensitivity.

During thruster burns hydrazine, hydrazine + water will be plumed. Hydrazine Hydrate ($N2H4+H2O$) has an absorption line at around 9.1µm11 so that it is understandable that sensitivity degradation is significant [15]. Also sensitivity degradation of Band 12 is much

significant in comparison to the other bands. Therefore, it is confirmed that hydrazine hydrate contaminated at the optics surface TIR as well as VNIR and SWIR.

Band No.	Wavelength
10	8.125 ~ 8.475µm
11	8.475 ~ 8.825µm
12	8.925 ~ 9.275µm
13	10.25 ~ 10.95µm
14	10.95 ~ 11.65µm

TABLE 1: Spectral channels of ASTER/TIR

3. CONCLUDING REMARKS
Due to the fact that dark signal and shot noise as well as circumstances of the VNIR such as detector temperature are stable so that detector of the VNIR is stable. Calibration lamp radiance monitor of photodiode output is stable so that calibration lamp is stable. Optics entrance monitor of photodiode which measures calibration lamp radiance shows a remarkable degradation. It was terminated 370 days after the launch, though. The degradation trend is almost same as OBC/RCC degradation (VNIR sensitivity degradation) if exterpolated degradation of optics entrance calibration radiance is compared to OBC/RCC. VNIR optics transparency is not so degraded. One of the possible causes of OBC/RCC degradation comes from contamination or ultra-violet light polymerization on the surface of VNIR optics entrance.

Assumption of which RCC degradation is caused by contamination of optics entrance of VNIR due to plume impingement from gas jet for attitude control seems to be reasonable. Sticking fraction of hydrazine is 0.1 while absorption coefficients at 500, 600, 700nm are 0.4, 0.3, 0.2%. Vicarious calibration shows difference sensitivity degradations between VNIR Band 3N and 3B. This may be caused by the fact that the optics for Band 3N is pointing to nadir while for Band 3B is pointing to 27.6 degree off-nadir because contamination situation due to thruster plume is different each other. Optics component are same for Band 3N and 3B so that both of the ultra-violet light polymerization and the sticking hydrazine hydrate are suspected. Similarly, MODIS sensitivity degradation shows a coincidence to VNIR OBC/RCC trend in terms of three obvious epochs on 520, 900 and 1400 days after the launch.

These three epochs are similar to the fuel consumption epochs. Using wavelength dependency of RCC degradation, size distribution is estimated with the relation between ln(wavelength) and ln(RCC degradation) based on power low distribution function. It has to be validated though. In a realistic case, thruster plume sticks to the optics but not situated as a particle. There is an evidence of sticking hydrazine hydrate on the TIR optics due to the fact that absorption wavelength of hydrazine hydrate corresponds to the most significant sensitivity degradation band of TIR. Consequently, optics transparency would be a most suspected cause of the RCC (sensitivity) degradation due to plume impingement by hydrazine hydrate from the thrusters or ultra-violet light polymerization of optics. Further investigation is needed.

4. REFERENCES
[1]   Arai K., Preliminary assessment of radiometric accuracy for MOS-1 sensors, International Journal of Remote Sensing, 9, 1, 5-12, 1988.

[2]   Barker, J.L., S.K. Dolan, et al., Landsat-7 mission and early results, SPIE, 3870, 299-311, 1999.

[3]   Barnes, R.A., E.E.Eplee, et al., Changes in the radiometric sensitivity of SeaWiFS determined from lunar and solar based measurements, Applied Optics, 38, 4649-4664, 1999.

[4]   Gellman, D.I., S.F. Biggar, et al., Review of SPOT-1 and 2 calibrations at White Sands from launch to the present, Proc. SPIE, Conf.No.1938, 118-125, 1993.

[5]   Ungar S.G., E.M. Middleton, L. Ong, P.K.E. Campbell, EO-1 Hyperion onboard performance over eight years: Hyperion Calibration,
http://eo1.gsfc.nasa.gov/new/SeniorReviewMaterial_References.doc

[6]   Hagolle, O., P.Galoub, et al., Results of POLDER in-flight calibration, IEEE Trans. On Geoscience and Remote Sensing, 37, 1550-1566, 1999.

[7]   Sakuma F., A.Ono, M.Kudoh, H.Inada, S.Akagi, and H.Ohmae, ASTER on-board calibration status, Proc. SPIE, 4881, 407-418, 2002.

[8]   Thome, K., K. Arai, S.Tsuchida, S.Biggar, Vicarious Calibration of ASTER via Reflectance-Based Approach, IEEE Trans. on Geoscience and Remote Sensing, 46, 10, 2008.

[9]   Daniela Dirtu, Lucia Odochian, Aurel Pui, Ionel Humelnicu, Thermal decomposition of ammonia. N2H4 –an intermediate reaction product, Central European Journal of Chemistry, DOI: 10.2478/ s11532-006-0030-4, 2006.

[10] During, J.R., S.F. Bush and E.E. Mercer: "Vibrational spectrum of hydrazine and a Raman study of hydrogen bonding in hydrazine", The J. Chem. Physics", 44, 11, 4238–4247, 1966.

[11] Itoh, N., M.Katoh, N.Okano, Comparison of spectral transmittance degradation due to organic gas contamination with on-orbit degradations of launched sensors, Proceedings of SPIE, 7149, 7149F, 2008.

[12] Arai, K., N.Ohgi, H.Inada, Suspected plume impingement onboard calibration system of Terra/ASTER investigated through trend analysis onboard calibration data, Proceedings of the ISPRS Commission VIII, WG VI/4, 2010.

[13] Kohei Arai,Nagamitsu Ohgi, Fumihiro Sakuma, Satoshi Tsuchida, Hitomi Inada, Trend analysis of onboard calibration data of Terra/ASTER/VNIR and one of the suspected causes of sensitivity degradation, Proceedings of the Conference on Characterization and Radiometric Calibration for Remote Sensing (CALCON 2010), 2010.

[14] X. Xiong, A. Wu, J. Esposito, J. Sun, N. Che, B. Guenther, W. Barnes, Trending Results of MODIS Optics On-orbit degradation , *Proceedings of SPIE Earth Observing Systems VII*,4 814, 2002.

[15] Sakuma F., M.Kikuchi, N.Ohgi, and H.Ono, ASTER TIR sensitivity degradation and hydrazine, Proceedings of the 49th General Assembly of the Remote Sensing Society of Japan, 2010.

Method for Estimation of Damage Grade and Damaged Paddy Field Areas Due to Salt Containing Sea Breeze with Typhoon Using Remote Sensing Satellite Imagery Data

Kohei Arai   *arai@is.saga-u.ac.jp*
Information Science Department
Saga University
Saga City, 840-8502, Japan

Abstract

Methods for estimation of damage grade and damaged paddy field areas due to salt containing sea breeze with typhoon using remote sensing satellite imagery data is proposed. Due to a fact that Near Infrared: NIR camera data is proportional to vitality of vegetation, it is possible to estimate damage grade and damaged paddy field areas due to salt containing sea breeze with typhoon using NIR channels of remote sensing satellite imagery data. Through regressive analysis between measured and estimated damage grade and damaged paddy field areas, it is found that there is a good correlation between both. Also it is found that there is a proportional relation between salt amount attached to the rice crop leaves and NIR reflectance measured with NIR channels of remote sensing satellite imagery data. Thus it is validated the proposed estimation method for damage grade and damaged paddy field areas due to salt containing sea breeze with typhoon using NIR channels of remote sensing satellite imagery data.

Keywords: Typhoon Disaster, NIR Radiometer Onboard Satellite, Damage Due to Salt Containing Sea Breeze.

1. INTRODUCTION

Vegetation vitality can be monitored with Near Infrared: NIR of spectral reflectance measured by ground based and satellite based instruments [1]. Also Normalized Difference Vegetation Index is very useful index for representing vegetation vitality [2]. For instance, NDVI can be calculated with the following simple equation, $NDVI=(IR-R)/(IR+R)$ where R denotes reflectance of vegetation in the red wavelength region while IR denotes reflectance in NIR region, respectively. NDVI was originally used as a measure of green biomass [3]. It got a solid theoretical basis as a measure of the solar photosynthetically active radiation absorbed by the canopy [4],[5]. Its application is limited, though, by a complexity of interacting factors involved in the formation of the reflectance response (see, for review [6]-[10]).

The method proposed here allows vegetation damage grade and damaged area estimations based on the NDVI as well as NIR reflectance. In particular, an estimation method of damage grade and damaged paddy field areas due to salt containing sea breeze with typhoon using NIR reflectance of remote sensing satellite imagery data is proposed. Also salt amount which is attached to the rice crop leaves is attempted for estimation. Through regressive analysis, a relation between NDVI and salt amount is clarified then a regressive equation which allows calculation of salt amount using NDVI is developed. The paper also describes trend analysis of the damage grade and damaged areas using satellite imagery data. Spatial distribution can be analyzed with satellite imagery data together with quantitative analysis. Also time series of analysis of damage grade and damaged area can be made with satellite imagery data.

The following section describes the detailed method for damage grade and damaged area estimation with satellite imagery data and time series analysis followed by examples of damage

grade and damaged area estimation due to salt containing sea breeze caused by typhoon together with time series analysis. Finally, conclusions with some discussions are followed.

2. PROPOSED METHOD

2.1 Damaged Vegetated Area Estimation Due to Salt containing Sea Breeze With Vegetation Vitality Measurement

Damaged vegetated area due to salt containing sea breeze of typhoon can be estimated through a comparison of NDVI which is derived from two remote sensing satellite imagery data which are acquired on before and after the typhoon pass. Also damage grade can be estimated with NDVI as well. Because one of the greatest reason of damage is caused by sea salt which is contained in sea breeze caused by typhoon, so that the relation between attached salt amount to vegetation and damage grade has to be clarified. Due to the fact that vegetation vitality is getting worth in accordance with attached salt amount remarkably, it is considered that there is an exponential relation between both, not a proportional relation. Therefore exponential regressive analysis is proposed for representation of the relation between both.

2.2 Time Series Analysis

Even if the attached salt amount is same, vegetation damage grade will be increased for time being. By using NDVI derived from remote sensing satellite imagery data, damage grade is estimated. Then relation between vegetation damage grade and duration time is estimated with time series of remote sensing satellite imagery data. Such this trend analysis method is proposed for time series of vegetation damage grade analysis.

3. EXPERIMENTS

3.1 Example of Typhoon Which Hit the Northern Kyushu, Japan on 10 September 2006

The typhoon number 13 in 2006 was borne at the ocean in south eastern offshore of Philippine at around 21:00 local time on September 10. It grew up and moved to northwest direction. After the typhoon was passing through Ishigakijima Island, Japan on September 16 with atmospheric pressure of 919 hPa and maximum wind speed of 55 m /s then it changed its direction to northeast direction and finally reached to Kyushu Island, Japan. Then the typhoon landed on Sasebo city in Nagasaki prefecture, Kyushu, Japan at 18:00 local time on September 17 with maximum wind speed of 40 m/s. After that it moved to Genkainada offshore through Fukuoka city at 20:00 local time on that day. Figure 1 shows the typhoon track with the time duration.

Agricultural damage in Saga prefecture, for instance, was more than 12 billion Japanese Yen which was occurred in mainly rice crop and soybeans in the reclaimed farm lands near coastal regions. This was mainly caused by salt containing sea breeze. Severe storm of typhoon hit the Saga prefecture at the same time of high tide so that the coastal areas in the Chikushi plane in Kyushu Island was damaged by the typhoon 13 due to salt containing sea breeze. Furthermore, it was fine days after the typhoon hit so that damaged areas expanded to street tree areas and mountainous areas.

Approximately 80 percent of the rice crop farm area (23,400 ha) was damaged (Total rice crop farm area was 29,000 ha in 2006). The server damaged area, in particular, was 15,800 ha, about half of the total rice crop farm area. Figure 2 shows local government reported contour lines for more than 70 %, between 30-70%, less than 30% damaged areas borders.

Black colored contour line (more than 70% areas was damaged) is situated on the rout number 444. There are street trees along with the rout number 444 so that vegetation damage due to salt containing sea breeze at rear side of the street trees is quite different from the area which is situated on the other side, fore side of the street trees. This situation is same for the border line of rout number 207 and 264. There is the pink colored border line along with the routs. Then the red line is corresponding to the rout number 34.
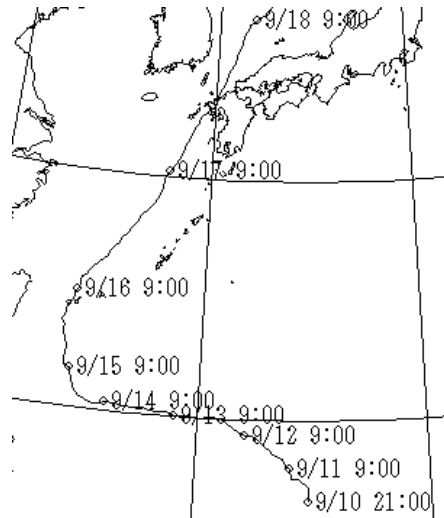
FIGURE 1: Typhoon track of the typhoon number 13 in 2006

FIGURE 2: Contour lines of borders for Black line: more than 70 %, Pink line: between 30-70%, Red line: less than 30% damaged areas

3.2 Damaged Area Estimation With Remote Sensing Satellite Imagery Data

SPOT/HRV[1] imagery data which were acquired on August 25 (before the typhoon number 13 hit) and September 23 (just five days after the typhoon hit) are shown in Figure 3. Also spectral response of SPOT/HRV of multispectral bands is shown in Table 1.

---

1 Spatial resolution of High Resolution Visible: HRV sensor onboard SOPT satellite developed by CNES (French Space Agency) and operated by SPOT Image Co., Ltd is 10 m for multi-spectral mode.
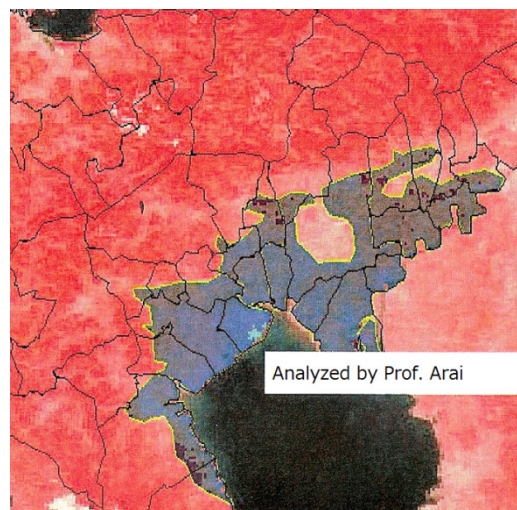
(a) August 25   **(b) September 23**
FIGURE 3 SPOT/HRV image which were acquired on August 25 and September 23 2006.

Mode	Band	Wavelength (μm)	Resolution (m)
Multispectral	XS1	0.50 - 0.59 (Green)	20
Multispectral	XS2	0.61 - 0.68 (Red)	20
multispectral	XS3	0.79 - 0.89 (Near IR)	20

TABLE 1: Spectral response of the SPOT/HRV of multispectral bands

Red colored areas show well vegetated areas while grey or blue colored areas show urbanized areas.. Almost farm areas in SPOT/HRV image of August 25 show vital and well vegetated areas while the portion of areas changed the colored from red (vital) to blue (week vegetation) in SPOT/HRV image of September 23.. These areas are damaged areas obviously due to salt containing sea breeze of typhoon number 13. By comparing both SPOT/HRV images, these areas are extracted. Figure 4 shows the extracted vegetation damaged areas.

Analyzed by Prof. Arai

FIGURE 4: Vegetation damaged areas extracted through the comparison between SPOT/HRV images which were acquired on August 25 and September 23 2006.

One of insitu data of attched salt on the rice crop leaves (salt amount in unit of mg / leaf)is illustrated in Figure 5. Figure 5 also shows the contour lines for which salt amount   a leaf is less than 0.5 mg/leaf, 0.5-1.0 mg/leaf, 1.0-1.5 mg/leaf, 1.5-2.0 mg/leaf and greater than 2.0 mg/leaf, respectively.
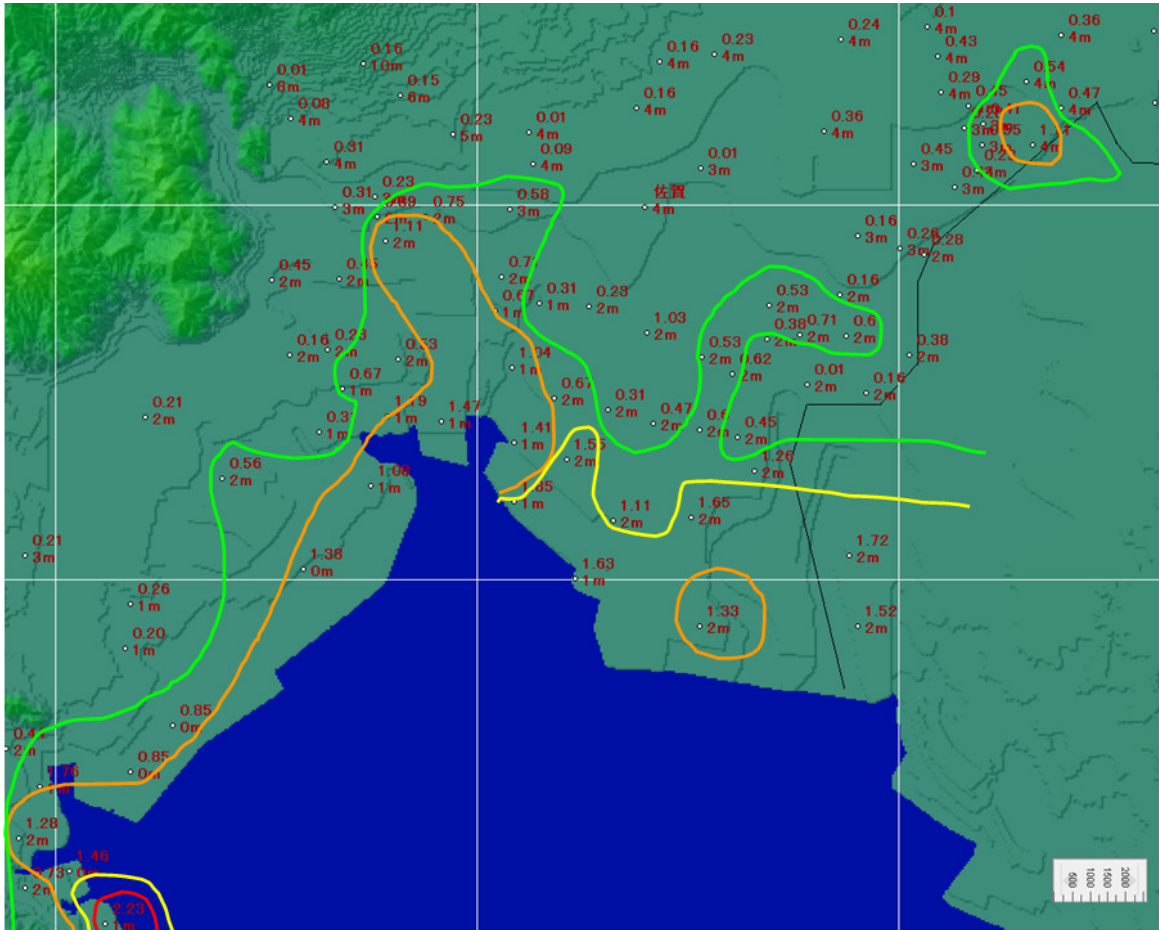
FIGURE 5: Attached salt amount to rice crop leaves (the top number) and elevation at that locations (the bottom number) as well as contour lines for which salt amount   a leaf is less than 0.5 mg/leaf, 0.5-1.0 mg/leaf (green), 1.0-1.5 mg/leaf (orange), 1.5-2.0 mg/leaf (yellow) and greater than 2.0 mg/leaf (red), respectively.

One of the specific features of these contour lines is that attached salt amount rich areas area situated along with the rivers. This implies that salt containing sea breeze of typhoon blew from the south (the Ariake Sea) to the north (mountainous areas) along with the rivers. Therefore, attached salt amount is significant at the regions which are situated at the valley associated with the rivers even if the regions are situated far from the coastal region. Figure 4 and 5 show a coincidence in terms of damaged areas and the attached salt amount.

3.3 Regressive Analysis
As is shown in Figure 5, there is a relation between salt amount attached to the damaged rice crop leaves and vegetation vitality which is derived from satellite imagery data, NDVI. By using all the insitu data of salt amount and calculated NDVI with the corresponding pixel of the insitu data

Kohei Arai

location, regressive analysis was conducted. By using SPOT/HRV imagery data, NDVI of corresponding to the insitu locations with 20m by 20m areas can be calculated. Figure 6 shows the relation between SPOT/HRV 20m derived NDVI and insitu data of salt amount attached to the rice crop leaves. Because the vegetation vitality is significantly decreased in accordance with increasing of salt amount, empirical equation of the relation would be a linear function. Then regressive analysis with a linear function is conducted with the equation (1).

$$S = a\,N + b \qquad\qquad\qquad\qquad\qquad\qquad (1)$$

where S, N denote Salt amount (Salinity) attached to the rice crop leaves (mg/leaf), Normalized Difference Vegetation Index (NDVI) while a and b denote regressive coefficients. The results from the regressive analysis show a=0.0223, b=-1.789 and correlation coefficient R square value is 0.6. Although mean of the salt amount is 0.607, standard deviation of the salt amount is comparatively large, 0.505 while that of the NDVI is 17.51 (mean of the NDVI is 107.33). It is because that the location of insitu data of salt amount is not always the center of SPOT/HRV 20m pixel. Also situations of rice crops are different each other location. Namely, topological feature, shadow influences, illumination condition, soil condition, weather condition, etc. are different each other location.
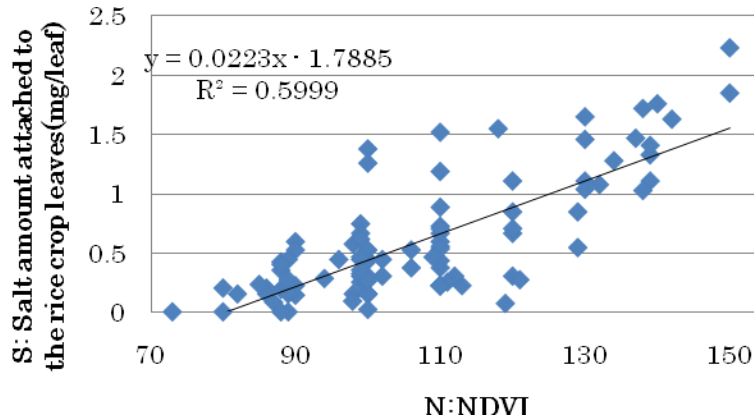
FIGURE 6 : Relation between NDVI derived from MODIS 250m and the correspoding location of insitu data of salt amount attached to the rice crop leaves.

3.4 Time Series Analysis
Two different spatial resolution of satellite imagery data are used for time series analysis. One is SPOT/HRV (High Resolution Visible) with 10m of spatial resolution and the other one is MODIS (Moderate Resolution of Imaging Spectrometer) on both satellites of Terra and Aqua with 250 m of spatial resolution. Characteristics of MODIS 250m of Leve-1B products are shown in Table 2.

Primary Use	Band	Bandwidth (nm)	Central Wavelength (nm)	Pixel Size (m)
Land/Cloud/Aerosols	1	620 - 670	645.5	250
Boundaries	2	841 - 876	856.5	250

TABLE 2: Characteristics of MODIS 250m of Level 1B data products

Acquisition dates are as follows,

Kohei Arai

SPOT/HRV: 25 August (Figure 3(a)), and Figure 7 of 20 September and 23 September (Off-nadir observation)
Terra/MODIS: Figure 8 of 24 August, 7 September, 20 September, 28 September, 19 October
Aqua/MODIS: 8 September, 26 September

The SPOT/HRV which was acquired on the closest time before the typhoon hit the Kyushu Island, Japan was acquired at 11:08 local time on 25 August while that of MODIS was acquired at 10:58 on 24 August 2006. Meanwhile, the SPOT/HRV which was acquired on the closest time after the typhoon hit the Kyushu Island, Japan was acquired at 11:18 local time on 20 September, just three days after the typhoon hit, while that of MODIS was acquired at 10:58 on 20 September 2006. By comparing the SPOT/HRV and MODIS imagery data which are acquired on the dates before and after the typhoon hit, damaged vegetation area and damage grade can be evaluated. Also once the regressive equation is created with the aforementioned SPOT/HRV and MODIS data together with the insitu data of attached salt on the vegetation, then trend analysis of damage grade can be done with the time series of the aforementioned MODIS data.
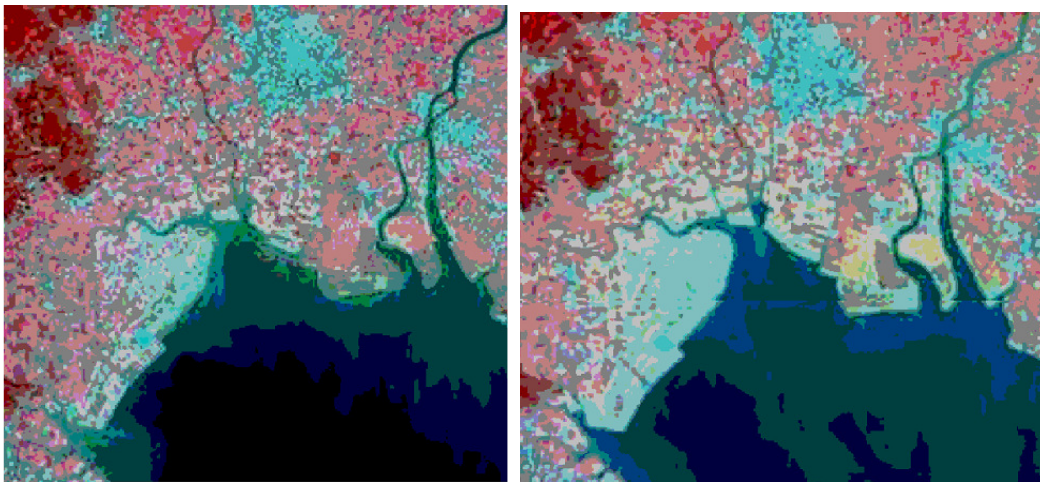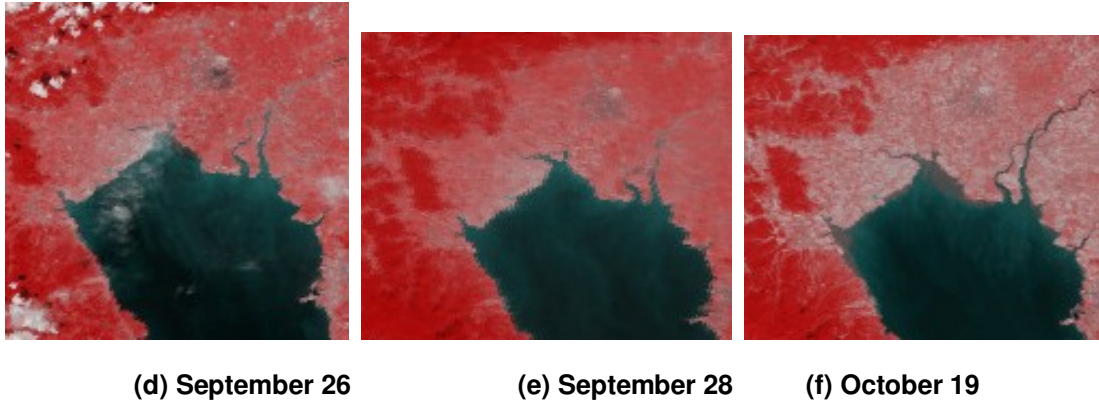

FIGURE 7 : Extracted and damaged area (light blue colored areas) with the enhanced SPOT/HRV images which were acquired on September of 20 (left) and 23 (right) 2006.
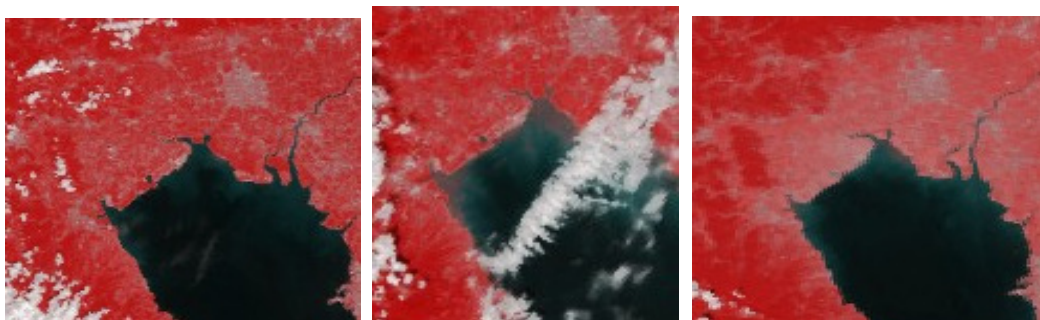
(a) **August 25**　　　　(b) **September 7**　　　　(c) **September 20**

(d) September 26   **(e) September 28**   **(f) October 19**

FIGURE 8 Time series of MODIS data of Saga, Japan.

Fine days were continued a couple of weeks after the typhoon hit the Saga prefecture so that damaged areas was getting larger even for three days, as is shown in Figure 7. Damaged paddy field areas due to attached salt to the rice crop leaves got expanded around 34 % during three days, from September 20 to 23 2006 in comparison between two SPOT/HRV imagery data of September 20 and 23 2006 which is shown in Figure 7. Figure 8 shows the time series of MODIS images of southern portion of Saga prefecture which were acquired on August 25, September 7 (before the typhoon number 13 hit), September 20, 26, 28 (after the typhoon number 13 hit), and October 19 2006 (after harvest other crops). The first two images show almost same vegetation vitality. Within 13 days, from August 25 to September 7, all kinds of crops were grown-up so that vegetation vitality was increased a little bit. Turns out, MODIS image of September 20 shows remarkably changes in vegetation vitality, in particular, paddy fields which are situated in the coastal areas of Ariake Sea. Pink colored areas show degraded areas in vegetation vitality. The color of the paddy fields which are situated in the Ariake Sea coastal areas changed from red to pink. This implies that these areas were damaged by salt containing sea breeze from the typhoon number 13. Since then, the damaged area was getting larger by the time by time, September 26, 28 2006. After the remains of rice cop removals and harvesting other types of crops in the middle of October, vegetation vitality of all of the farm areas goes down sharply as is shown in Figure 8.

4. CONCLUSIONS

The proposed method for estimation of damage grade and damaged paddy field areas due to salt containing sea breeze with typhoon using remote sensing satellite imagery data is validated through experiments with SPOT/HRV of satellite imagery data and insitu salt amount attached to rice crop leaves. Equation which represents the relation between salt amounts attached to rice crop leaves and SPOT/HRV derived NDVI is created through linear regression with 0.6 of R square value. Also time series analysis method for damaged areas estimation due to attached salt is validated with MODIS 250m of level 1B data products.

5. REFERENCES

[1] Ramachandran, Justice, Abrams Edt., Kohei Arai, et al., Land Remote Sensing and Global Environmental Change, Part-II, Sec.5: ASTER VNIR and SWIR Radiometric Calibration and Atmospheric Correction, 83-116, Springer 2010.

[2] Anatoly A. Gitelson,* Yoram J. Kaufman, + and Mark N. Merzlyak, Use of a Green Channel in Remote Sensing of Global Vegetation from EOS-MODIS, REMOTE SENS. ENVIRON. 58:289-298 (1996)

[3] Tucker, J. C. (1979), Red and photographic infrared linear combination for monitoring vegetation. *Remote Sens. Environ.*8:127-150.

Kohei Arai

[4]   Sellers, P. J. (1985), Canopy reflectance, photosynthesis and transpiration. *Int. J. Remote Sens.* 6:1335-1372.

[5]   Sellers, P. J. (1987), Canopy reflectance, photosynthesis and transpiration. II. The role of biophysics in the linearity of their interdependence. *Remote Sens. Environ.* 21:143-183.

[6]   Andrieu, B., and Baret, F. (1993), Indirect methods of estimating crop structure from optical measurements, In *Crop Structure and Light Microclimate. Characterization and Applications* (C. Varlet-Grancher, R. Bonhomme, H. Sinoquet, Eds.), INRA Edition, Paris, pp. 285-322.

[7]   Baret, F., and Guyot, G. (1991), Potential and limits of vegetation indexes for LAI and APAR assessment. *Remote Sens. Environ.* 35:161-173.

[8]   Curran, P. J., Dungan, J. L., Macler, B. A., and Plummer, S. E. (1991), The effect of a red leaf pigment on the relationship between red edge and chlorophyll concentration. *Remote Sens. Environ.* 35:69-76.

[9]   Horler, D. N., Dockray, M., and Barber, J. (1983), The red edge of plant leaf reflectance. *Int. J. Remote Sens.* 4(2): 273-288.

[10]   Huete, A. R., and Liu, H. Q. (1994), An error and sensitivity analysis of the atmospheric and soil correcting variants of the NDVI for the MODIS-EOS, *IEEE Trans. Geosci. Remote Sens.* 32:897-905.

Comparative Calibration Method Between Two Different Wavelengths With Aureole Observations at Relatively Long Wavelength

Kohei Arai   *arai@is.saga-u.ac.jp*
Information Science Department
Saga University
Saga City, 840-8502, Japan

Xing Ming Liang   *xingming.liang@noaa.gov*
Center for Satellite Application and Research (STAR),
NOAA/NESDIS,
Camp Springs, MD 20746, U.S.A.

Abstract

A multi-stage method for calibration of sunphotometer is proposed by combining comparison calibration method between two different wavelengths with aureole observation method for long wavelength calibration. Its effectiveness in reducing the influences for calibration due to molecular and aerosol's extinction in the unstable turbidity conditions is clarified. By comparing the calculated results with the proposed method and the existing individually calibration method, it is found that the proposed method is superior to the existing method in terms of calibration accuracy. Namely, Through a comparison between ILM and the proposed method using band 0.87um as reference, the largest calibration errors are 0.0014, 0.0428 by PM are lower than that by ILM (0.011,0.0489) for sky radiances with no error and -3~+3%, -5~+5% errors. By analyzing the observation data of 15 days with POM-1 Skyradiometer, the largest standard deviation of calibration constants by PM is 0.02016, and is lower than that by ILM (0.03858).

Keywords: Sunphotometer, Calibration, Langley Method, Modified Langley Method, Aureole, Solar Direct Irradiance, Solar Diffuse Irradiance.

1. INTRODUCTION

Sunphotometer have been applied widely to measure aerosol optical properties for analyzing local and global climate, such as Aerosol Robotic Network (AERONET)[1]. There are about 500 institutions of ground based aerosol monitoring by sunphotometers or skyradiometers in the AERONET. Thus, the maintenance of the calibration constants of sunphotometers is essential in such works, especially for monitoring of long-term variations of atmospheric turbidity [1]-[9].

It is well known that the common Langley method (CLM) is inability to assure to obtain accurate calibration constant for sunphotometer due to the influence by unstable atmospheric extinction [10]-[13]. In the CLM, the calibration constant is obtained by extrapolation of the plot of the logarithm of the sunphotometer reading against atmospheric air mass to air mass 0. Large error of calibration constant, however, it will occur as the optical depth of atmosphere changes during the calibration period because of the unstable atmospheric turbidity. For this reason, many previous works which focus on reducing the influence due to the unstable atmospheric turbidity in the instrument calibration have been studied. One of the typical representatives is Improved Langley method proposed by T. Nakajima [13]. They introduced an analysis of volume spectrum to firstly estimate the aerosol optical depth in order to avoid the error due to the change of aerosol optical depth in accordance with the unsteady turbidity conditions. In consequence, it made a greater improvement for sunphotometer calibration than the common Langley method.

---

[1] **aeronet.gsfc**.nasa.gov/Operational/pictures/.../Cimel_set_up.PDF

Some factors, however, such as observation errors in circumsolar radiances, the scattering of atmospheric molecular, the estimate errors of volume spectrum and the other assumptions of atmospheric conditions, result in insufficiency to reduce the contribution of multiple scattering by analysis of volume spectrum. Sometime estimation errors of aerosol optical depth are also significant. Thus the estimation accuracy of the calibration constants also becomes small by ILM, especially for the short wavelength. On the other hand, ratio Langley method (RLM), proposed by B.W. Forgan (1994) [12], is the method which is depend on a known calibration for a reference wavelength to permit calibration at the others. Using this method, it is possible to improve calibration accuracies by selecting the long wavelength with being calibrated well by ILM as a reference to perform calibration at the others.

In the following section, a multi-stage calibration method by combining ILM with RLM to perform calibration for sunphotometer is proposed. Results from a numerical simulation and an analysis for the actual data measurement by skyradiometer are followed by in order to validate the proposed method. Then conclusions and some discussions are followed.

2. ANALYSIS OF VOLUME SPECTRUM AND IMPROVED LANGLEY METHOD

The CLM is based on the Beer-Lambert law as follows,

$$\ln F = \ln F_0 - m\tau \tag{1}$$

where F and F_0 are solar downward irradiances at surface and extra-atmosphere, respectively. τ is total optical depth of atmosphere. m is atmospheric air-mass, is approximately equal to $1/\cos(\theta_0)$ as θ_0 (solar zenith angle) is less than $75^\square$. Invariance of the aerosol optical depth in accordance with stable atmospheric condition at different solar zenith angles is necessary to estimate high accurate solar constant in CLM. But, it is difficult to satisfy the temporal stability of atmosphere in usual locations, except for some special region, such as high elevation of mountain. A sensitivity analysis for calibration in different aerosol models have been performed by M.Tanaka (1986) [11], and there were about 2.6~10% retrieval errors of the calibration constants by means of CLM as the aerosol optical depth varies based on a parabolic variation corresponding changes with the extent of ±10%.

To remove the influence due to variant optical depth of aerosol in accordance with the unsteady turbidity conditions during calibration period, T.Nakajima (1996) proposed an improved Langley method in which the calibration are performed by simultaneous measurements combining the direct-solar and circumsolar radiation [13]. The aerosol optical depth is estimated firstly by an analysis of volume spectrum (AVS). In this analysis, the circumsolar radiances are replaced by a relative intensity as equation (2).

$$R(\theta) = \frac{F(\theta)}{Fm\Delta\Omega} = \omega\tau P(\theta) + q(\theta) \tag{2}$$

where, $R(\theta)$ is the relative intensity of circumsolar radiance, $F(\theta)$, and normalized by direct irradiance(F), approximate air mass (m) and the solid angle($\Delta\Omega$). ω is the single scattering albedo. $q(\theta)$ indicates the multiple scattering contribution. $P(\theta)$ is the total phase function of aerosols and molecules at scattering angle is θ and given by.

$$P(\theta) = (\omega_a \tau_a P_a(\theta) + \omega_m \tau_m P_m(\theta))/\omega\tau \tag{3}$$

where ω_a, τ_a and $P_a(\theta)$ are the single scattering albedo, the optical depth, and the phase function of aerosol, respectively; and ω_m, τ_m and $P_m(\theta)$ are corresponding quantities of air molecule. Assume the aerosol particle is sphere and homogeneous, by Mie theory, $\omega_a \tau_a P_a(\theta)$ and the aerosol optical depth can be defined as,

$$\omega_a \tau_a P_a(\theta) = \int_{r1}^{r2} K(\theta, kr, \tilde{m}) v(r) d\ln r \qquad (4)$$

$$\tau_a = \int_{r1}^{r2} K_{ext}(kr, \tilde{m}) v(r) d\ln r \qquad (5)$$

where $v(r) = (4\pi/3) r^4 n(r)$, $n(r)$ is columnar radius distribution of aerosol. $k = 2\pi/\lambda$, $\tilde{m} = n - i\xi$ is refractive index, $K_{ext}(kr, \tilde{m})$, $K(\theta, kr, \tilde{m})$ are kernel functions and can be calculated by Mie theory. Using an inversion scheme of solving radiative transfer equation to correct repeatedly the multiple scattering contribution, $q(\theta)$ [4], an approximate solutions of volume spectrum, $v(r)$, can be estimated by circumsolar radiances. Then the aerosol optical depth also can be estimated by equation (5). Thus, equation (1) can be rewritten by

$$\ln F + m(\tau_m + \tau_o) = \ln F_0 - m\tau_a \qquad (6)$$

where τ_o is ozone optical depth, and the calibration constants can be obtained by extrapolation of the plot of the left item against $m\tau_a$ to $m\tau_a = 0$. This method is referred to Improved Langley Method (ILM). Because most of influence due to variant optical depth of aerosol in accordance with the turbidity atmosphere can be estimated by circumsolar radiances, the estimation accuracies of calibration constants will be improved conspicuously comparing with the CLM, with the plot of $\ln F$ against m.

On the other hand, the influences due to the small extent (θ<30°) of the circumsolar radiation, the scattering of atmospheric molecule, the observation errors of circumsolar radiances, the estimate errors of the volume spectrum and the other assumptions of atmospheric conditions, result in insufficiency to reduce the contribution of multiple scattering in solving radiative transfer equation by inversion scheme (T. Nakajima, 1996) [13]. Some errors will occur in estimation of the aerosol optical depth by AVS. Thus it is hardly assured to estimate the aerosol optical depth accurately for every wavelength of sunphotometer. Figure 1 shows the difference of the aerosol optical depth estimated by the AVS and by reanalysis of volume spectrum from skyradiometer measurement in several days.
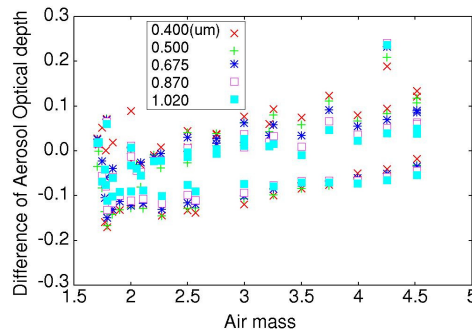
FIGURE 1: The Differences of aerosol optical depth by means of AVS and reanalysis of volume spectrum from air-mass 1.5 to 4.5. Data are observed by POM-1 of Skyradiometer[2] in 11/26/2003, 12/03/2003 and 12/04/2003 at Saga, Japan

It is found that the differences of aerosol optical depth between the estimation by AVS and by reanalysis sometime are larger than 10%. It means that the estimate accuracies of calibration constants can become low by ILM.

3. THE PROPOSED METHOD

From Figure 1, it is also found that the differences of aerosol optical depth in long wavelength are small than that in the shorts. This is because the influences due to the multiple scattering in the long wavelength are smaller, and the optical depth can be estimated accurately. This also means that the estimate accuracies of the calibration constants are higher in long wavelengths than that in the shorts. On the other hand, Ratio Langley method, proposed by B.W. Forgan (1994) [12], is the method which is depend on a known calibration for a reference wavelength to permit calibration at the others by assuming the relative size distribution of aerosol to remain constant as equation (7), so that the ratio of aerosol optical depth between the different wavelengths are assure to be constant as equation (8).

$$\tau_a(\lambda, t) = \pi A(t) \int K_{ext}(r, \lambda) f(r) d \ln r \qquad (7)$$

$$\tau_a(\lambda_1, t) / \tau_a(\lambda_2, t) = \tau_a(\lambda_1, t_0) / \tau_a(\lambda_2, t_0) = \psi \qquad (8)$$

where $f(r)$ is the relative size distribution that is dependent only on particle radius r, and $A(t)$ is the multiplier necessary to produce the correct size distribution at some time t. Thus the calibrations at the other wavelengths can be performed by using the reference wavelength as equation (9).

$$\ln F(\lambda_1) + m(\tau_m(\lambda_1) + \tau_o(\lambda_1)) = \ln F_0(\lambda_1) - \psi m \tau_a(\lambda_0) \qquad (9)$$

where λ_0, λ_1 are the reference wavelength and the calibrated wavelength, respectively. ψ is a constant. Because $m\tau_a(\lambda_0)$ has been calibrated well, it is calculated accurately $\ln F_0(\lambda_1)$ by least square regression for equation (9) between the left item and $m\tau_a(\lambda_0)$. It is possible to improve calibration accuracies by selecting the long wavelength with being calibrated well by ILM as reference to perform calibration at the others.

Therefore, a multi-stage calibration method is proposed. In the proposed method, accurate calibration constants in the long wavelength which are estimated by ILM are used. Also it is used as a reference to that at the other wavelengths. Because the ILM does work well in the code of Skyrad.pack, developed by T.Nakajima (1996) [4], this code will be used in our algorithm. The proposed process flow is shown in Figure 2.

---

[2] It is similar to the Aureolemeter for AERONET which is manufactured by Prede Co. Ltd.
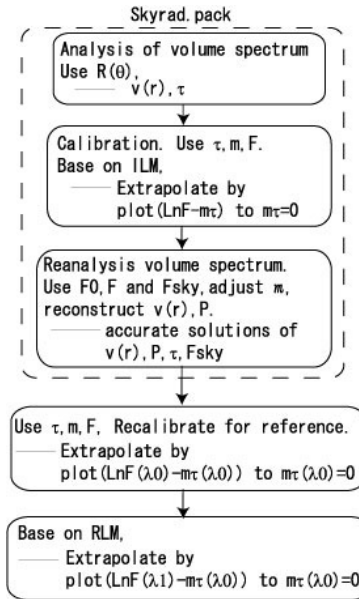
FIGURE 2: The algorithm of multi stage calibration method.

Firstly, the code Skyrad.pack.v42 is introduced in our algorithm. It includes three processes, level 0, calibration and level 1. In the level 0, based on AVS, the aerosol optical depth and the volume spectrum are approximately estimated by the circumsolar radiation. In the calibration, the calibrations are performed by ILM. In the level 1, on the other hand, it is used as the calibration constants estimated by ILM, and then it is combined with the direct and sky radiances. Thus, more accurate solution of aerosol optical depth, aerosol volume spectrum, refractive index of aerosol can be estimated by reanalysis of volume spectrum. Consequently, it is used the aerosol optical depth which is estimated from the level 1, i.e. reanalysis of volume spectrum, instead of that from the level 0. Then it is performed a calibration for the reference wavelength selected to obtain more accurate calibration constants. Finally, based on RLM, the well-calibrated at the reference wavelength can be used for that at the other wavelengths.

4. NUMERICAL SIMULATIONS

A numerical simulation is conducted to check a validity of the proposed method by comparing to the ILM method. The wavelengths are selected 0.4, 0.5, 0.675, 0.87 and 1.02um in accordance with the POM-1 of Skyradiometer manufactured by Prede Co. Ltd. The reference wavelength is set at 0.87um. The simulated data is generated by the Skyrad.pack.v42. The aerosol size distributions are defined two modes of log-normal distributions (bi-modal) as follows

$$n(\ln r) = \sum_{i=1}^{2} \frac{C_i}{\sqrt{2\pi}\log\sigma_i} \exp(-\frac{(\log r - \log\overline{r_i})^2}{2\log^2\sigma_i}) \tag{10}$$

where *n(lnr)dlnr* is the number density of particles between radii *r* and *r+dlnr*. The values of C_i is set as 1, and σ_i, $\overline{r_i}$ are set as same as the aerosol type observed at Saga, Japan in 2003. The set of parameters are shown in Table 1.

No mode	Ci	ri(um)	σi
1	1.0	0.37	1.95
2	1.0	3.06	2.36

TABLE 1: The parameters for log-normal distribution.

The refractive index of aerosol is set $m=1.50-0.01i$. Solar irradiance of extra-atmosphere is set 1.0. The variation of the optical depth of aerosol with time is given as follows (Shaw, 1976) [14].

$$\tau_a = \tau_{a0}(1 + \alpha t^2) \tag{11}$$

where τ_{a0} is aerosol optical depth at noon, and are set 0.1 and 0.2. α is assumed to be 0.011.

So that the aerosol optical depth changes in the extent of 0~20% of τ_{a0} as the air-mass vary from 1.5 to 4.5. We set 0,-3~3%,-5~5% random errors for the sky radiances to evaluate the calibration accuracies by ILM and the proposed method (PM). Figure 3 (a) and (b) shows the estimate errors of aerosol optical depth by AVS and reanalysis of volume spectrum for the wavelengths 0.4, 0.5 and 0.87μm with no error in sky radiances.

From this Figure, it may be concluded that,
(1) Estimate accuracies of the aerosol optical depth by reanalysis of volume spectrum are almost better than that by AVS,
(2) Estimate errors of aerosol optical depth in band 0.87μm are smaller than that in 0.4 and 0.5μm. Similarly, the cases with -3~3% and -5~5% errors in sky radiances, also can be concluded the same points as above.

Table 2(a), (b), (c) show that the comparisons of estimate accuracies of calibration constants by ILM and PM for the aforementioned five wavelengths. From the table, it is found that the calibration accuracies are higher by PM, especially in short wavelength 0.4μm.

To evaluate the influence of calibration accuracies due to changing of the relative size distribution, it is set σ_i and $\bar{r}_i$ ±3% and ±5% change in equation (10). The calibration results are shown in Table 3. From the table it may say that the calibration accuracies of the proposed method are higher than that of PM in ±3% change.

5. VALIDATION THROUGH OBSERVATIONS

It is also validated the proposed method by analysis of observation data from POM-1 of Skyradiomater. The POM-01 Skyradiometer can measure the direct, diffuse solar irradiance as well as aureole in solar almucantar and in the principal plane. It consists of the seven filters which the central wavelengths are at 0.315, 0.40, 0.50, 0.675, 0.870, 0.94 and 1.02μm. The filters of the wavelength center at 0.315μm and 0.94μm are used for estimation of O_3 concentration and precipitable water, respectively. The other filters are used for aerosol optical depth measurements. The instrument is acquired with a 0.5□half angle field of view. The instrument is located at Saga University, and observations were performed from September 2003 to May 2004. Data of 15 days are selected; these days are cloud-free.

(a)   (b)
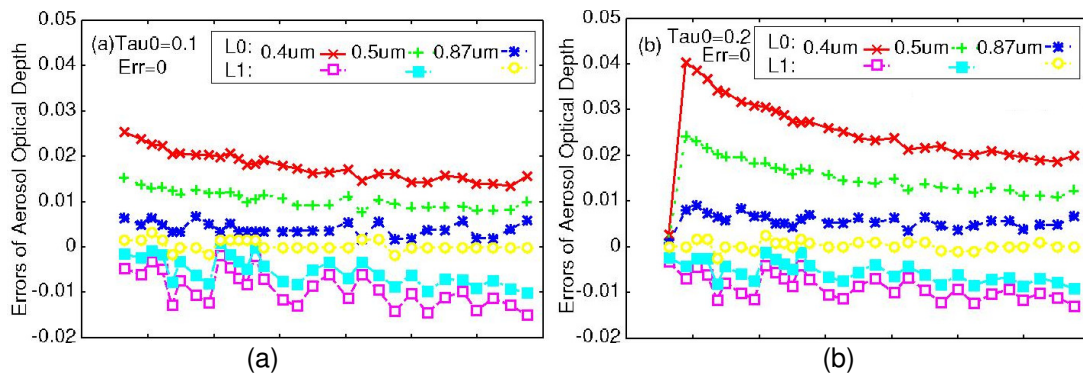
FIGURE 3: The estimation errors of aerosol optical depth by the method of AVS and the method through reanalysis of volume spectrum at the wavelength of 0.4, 0.5, and 0.87μm without any error in sky radiance measurement.

The Figure 4 shows the calibration constants at the reference wavelength estimated by ILM in the 15 days. It is found that the accuracies are high enough with the standard deviation of only 1%.
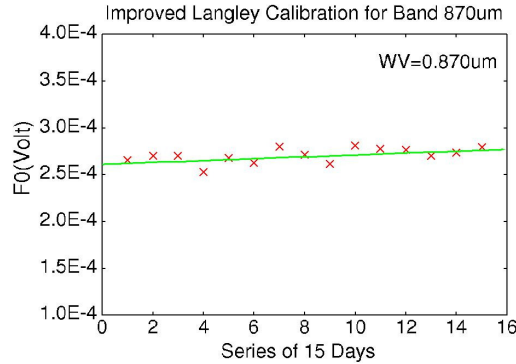
**FIGURE 4:** Calibration for the reference wavelength by ILM

The calibration results of ILM and PM methods are shown in Figure 5 (a) and (b) and Table 5. Figure 5 (a) shows calibration coefficient for the wavelength of 0.4μm and 0.5μm, while Figure 5 (b) also shows calibration coefficient for 0.675μm and 1.02μm. Table 5 indicates the standard deviations for each band in 15 days. Consequently, it is found that the standard deviation of PM method is smaller than that of ILM method, especially at the wavelength of 0.4μm. This also means that the number of times of calibration required for PM is less than that for ILM to attain the same accuracies.

	0.1		0.2		0.3	
WV (um)	ILM	PM	ILM	PM	ILM	PM
0.4	0.0008	0.0006	0.0029	0.0009	0.013	0.0014
0.5	0.0003	0.0006	0.0015	0.0006	0.01	0.0009
0.675	0.0012	0.0005	0.0006	0.0006	0.005	0.0005
0.87	0.0002	0.0002	0.0001	0.0001	0.003	0.0004
1.02	0.0002	0.0002	0.0001	0.0001	0.002	0.0004

(a) No error in circumsolar radiances

	0.1		0.2		0.3	
WV (um)	ILM	PM	ILM	PM	ILM	PM
0.4	0.011	0.004	0.017	0.009	0.023	0.011
0.5	0.008	0.003	0.009	0.006	0.012	0.009
0.675	0.003	0.002	0.003	0.002	0.015	0.007
0.87	0.006	0.002	0.001	0.001	0.002	0.001
1.02	0.002	0.001	0.001	0.002	0.001	0.001

(b)-3%~3% random errors in circumsolar radiances

	0.1		0.2		0.3	
WV (um)	ILM	PM	ILM	PM	ILM	PM
0.4	0.013	0.007	0.015	0.005	0.027	0.014
0.5	0.006	0.006	0.005	0.004	0.011	0.01
0.675	0.003	0.003	0.003	0.003	0.007	0.005
0.87	0.001	0.001	0.002	0.001	0.001	0.001
1.02	0.001	0.001	0.002	0.001	0.001	0.002

(c)-5%~5% random errors in circumsolar radiances.

TABLE 2: Comparison of estimation error for calibration from ILM and the proposed method as the optical depth are 0.1, 0.2 and 0.3.

	standard deviation	
W V (um)	ILM	P M
0.4	0.03858	0.02016
0.5	0.02219	0.01691
0.675	0.01837	0.01295
1.02	0.01022	0.00938

TABLE 3: Comparison of the Standard deviations between ILM and PM.

(a) 0.4 and 0.5μm   **(b) 0.675 and 1.02μm**
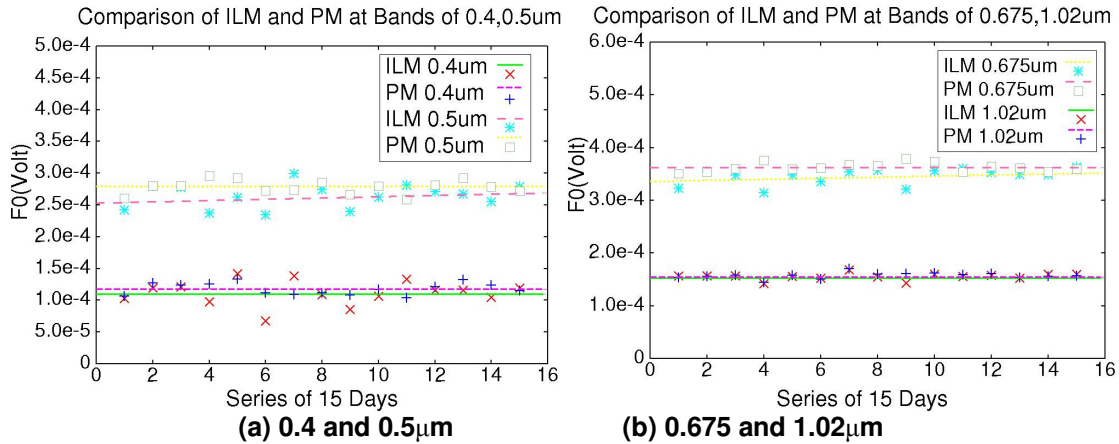
FIGURE 5: Calibration for 0.4μm and 0.5μm by ILM and PM.

6. CONCLUSIONS

A multi stage calibration method combining Improved Langley Method with Ratio Langley Method is proposed in this paper. From the numerical simulation, the estimation errors of aerosol optical depth result in calibration precision decrease by ILM. Through a comparison between ILM and the proposed method using band 0.87μm as reference, the largest calibration errors are 0.0014, 0.0428 by PM are smaller than that by ILM (0.011,0.0489) for sky radiances without any error and -3~+3%, -5~+5% errors. By analyzing the observation data of 15 days with POM-1 of Skyradiometer, the largest standard deviation of calibration constants by PM is 0.02016, and is smaller than that by ILM (0.03858). Thus it may say that the proposed calibration method is superior to the other conventional methods.

7. ACKNOWLEDGEMENTS

8. REFERENCES

[1]   Ramachandran, Justice, Abrams(Edt.),Kohei Arai et al., Land Remote Sensing and Global Environmental Changes, Part-II, Sec.5: ASTER VNIR and SWIR Radiometric Calibration and Atmospheric Correction, 83-116, Springer 2010.

[2]   Arai, K, Fundamental theory of remote sensing, Gakujutsu-Tosho-Shuppan Co. Ltd., 2001.

[3]   Arai, K. Self learning on remote sensing, Morikita-Shuppan Co. Ltd., 2004.

[4]   Arai, K., X.M. Liang, Simultaneous estimation of aerosol refractive index and size distribution using solar direct, diffuse and aureole based on simulated annealing, Journal of Remote Sensing Society of Japan, 23, 1, 11-20, 2003.

[5]   Arai K., X.M. Liang, Estimation method for Top of the Atmosphere radiance taking into account up and down welling polarization components, Journal of Japan Society of Photogrammetry and Remote Sensing, 44, 3, 4-12, 2005.

[6]   Liang X.M., K.Arai, Simultaneous estimation of aerosol refractive index and size distribution taking into account solar direct, diffuse and aureole of polarization component, Journal of Remote Sensing Society of Japan, 25, 4, 357-366, 2005.

[7]   Arai K., X.M. Liang, Characterization of aerosols in Saga city areas, Japan with direct and diffuse solar irradiance and aureole observations, Advances in Space Research, 39, 1, 23-27, 2007.

[8]   Arai K., Y.Iisaka and X.M. Linag, Aerosol parameter estimation with changing observation angle of around based polarization radiometer, Advances in Space Research, 39, 1, 28-31, 2007.

[9]   Arai K., X.M. Liang, Improvement of calibration accuracy of skyradiometer which allows solar direct, aureole and diffuse measurements based on Improved Modified Langley, Journal of Japan Society of Photogrammetry and Remote Sensing, 47, 4, 21-28, 2008.

[10] Schotland, R.M., Lea, T.K., Bias in a solar constant determination by the Langley method due to structured atmospheric aerosol. Appl. Opt., 25, 2486-2491, 1986.

[11] Tanaka, M., Nakajima, T., Shiobara, M., Calibration of a sunphotometer by simultaneous measurements of direct-solar and circumsolar radiations. Appl. Opt., 25, 1170-1176, 1986.

[12]   Forgan, B.W., General method for calibrating sun photometers. Appl. Opt., 33, 4841-4850, 1994.

[13] Namajima, T., Tonna, G., Rao, R. et al. Use of sky brightness measurements from ground for remote sensing of particulate polydispersions. Appl. Opt. 35, 2672-2686, 1996.

[14] Shaw, G.E., Error analysis of multi-wavelength sunphotometry. Pure Appl. Geophys., 114, 1, 1976.

INSTRUCTIONS TO CONTRIBUTORS

International Journal of Applied Sciences (IJAS) is publishing articles in all areas of applied sciences. IJAS seeks to promote and disseminate knowledge in the applied sciences, natural and social sciences industrial research materials science and technology, energy technology and society including impacts on the environment, climate, security, and economy, environmental sciences, physics of the games, creativity and new product development, professional ethics, hydrology and water resources, wind energy. IJAS is an academic peer reviewed on-line international journal of broad appeal aimed at fast publication of cutting edge multidisciplinary research articles reporting on original research across the fields of pure and applied sciences.

To build its International reputation, we are disseminating the publication information through Google Books, Google Scholar, Directory of Open Access Journals (DOAJ), Open J Gate, ScientificCommons, Docstoc and many more. Our International Editors are working on establishing ISI listing and a good impact factor for IJAS.

The initial efforts helped to shape the editorial policy and to sharpen the focus of the journal. Starting with volume 2, 2011, IJAS appears in more focused issues. Besides normal publications, IJAS intend to organized special issues on more focused topics. Each special issue will have a designated editor (editors) – either member of the editorial board or another recognized specialist in the respective field.

We are open to contributions, proposals for any topic as well as for editors and reviewers. We understand that it is through the effort of volunteers that CSC Journals continues to grow and flourish.

IJAS LIST OF TOPICS
The realm of International Journal of Applied Sciences (IJAS) extends, but not limited, to the following:

- Agricultura
- Audio
- Automotive Engineering
- Biological
- Bombs
- Building officials
- Chemical
- Combat Engineering
- Cryogenics
- Domestic Educational Technologies
- Energy
- Engineering geology
- Entertainment
- Environmental Engineering Science
- Environmental technology
- Fire Protection Engineering
- Fishing
- Food Technology
- Health Safety
- Industrial Technology
- Machinery
- Marine Engineering
- Materials science and engineering
- Metallurgical

- Architectural
- Automotive
- Biochemical
- Biomedical
- Broadcast
- Ceramic
- Civil
- Construction
- Domestic appliances
- Domestic Technology
- Energy storage
- Enterprise
- Environmental
- Environmental Risk Assessment
- Financial Engineering
- Fisheries science
- Food
- Genetic
- Health Technologies
- Industry Business Informatics
- Manufacturing
- Material Sciences
- Medical Technology
- Microtechnology

- Military Ammunition
- Military Technology and equipment
- Motor Vehicles
- Naval Engineering
- Nutrition
- Ontology
- Optics
- Pharmaceuticals
- Sanitary Engineering
- Textile
- Traffic
- Visual Technology

- Military Technology
- Mining
- Music
- Nuclear technology
- Ocean
- Optical
- Particle physics
- Safety Engineering
- Space Technology
- Tissue
- Transport
- Zoography

CALL FOR PAPERS

Volume: 3 - **Issue:** 1 - February 2012

i. Paper Submission: November 30, 2011   **ii. Author Notification:** January 01, 2012

iii. Issue Publication: January / February 2012

CONTACT INFORMATION

Computer Science Journals Sdn BhD
B-5-8 Plaza Mont Kiara, Mont Kiara
50480, Kuala Lumpur, MALAYSIA
Phone: 006 03 6207 1607
006 03 2782 6991

Fax: 006 03 6207 1697

Email: cscpress@cscjournals.org